

Residual Stresses and Strains and Remodelling of Tissues

J. JOACHIM TELEGA and MACIEJ STAŃCZYK

*Institute of Fundamental Technological Research,
Polish Academy of Sciences,
ul. Świątokrzyska 21,
00-049 Warsaw, Poland
mstan@ippt.gov.pl*

The aim of these notes is to synthesize the available results on experimental data and mathematical modelling of residual stresses and strains in bone and soft tissues. Their role in bone and soft tissue remodelling is carefully discussed.

1. Introduction

During lifetime both bone and soft tissue undergo permanent changes dependent on many mechanical and biological factors like aging, nutrition, drugs. As a rule tissues are anisotropic and inhomogeneous. After a thought one intuitively feels that residual stresses should be present in bones and soft tissues. Surprisingly, their existence was shown relatively late, if one thinks of already long history of biomechanics of bone and soft tissues. We recall that residual stresses are the stresses which remain in material after unloading (no-load condition). We will use equivalently the notion “residual stress” or “initial stress”.

It seems that the first who showed existence of residual stress in bone were Ascenzi and Benvenuti [2]. These authors provided evidence that isolated osteonic lamellae are in a state of initial stress, cf. Section 2 of our paper. However, no estimation of magnitude of the stress was given. Such an attempt was undertaken in 1999 by Ascenzi [4].

From the historical perspective one should also mention the papers by Gebhardt [22] and Caglioti [7]. According to the first author the parallel but

opposite orientation of positive monoaxial birefringence of the collagenous fibres and the negative monoaxial birefringence of the calcified interfibrillar cementing substance should be attributed to a state of tension between these two components of the calcified bone, cf. Ascenzi and Benvenuti [2].

In his investigation on X-ray diffraction of bone, Caglioti [7] claimed that, in bone collagen, amino acids are kept under tension and held up by the apatite crystallites which are elongated and arranged parallel to the collagenous fibres.

In 1994, Tanka and Adachi [69] proposed a simple one-dimensional model for mechanical bone remodelling incorporating residual stress. These authors speculate about the existence of residual stress in bone by analogy with earlier discovered residual stress in soft tissue. Next, residual stress was examined for the leporine tibiofibula bone [70] and the bovine coccygeal vertebra [1, 70].

Residual stress in soft tissues was discovered several years later. According to Fung [18] residual stress in soft tissues were discovered independently by Vaishnav and Vossoughi in 1983 [76], and his former student P. Pattituci [52], who discovered such stress in left ventricle of a rabbit in 1982. The former authors investigated an aortic segment.

Currently attempts are made to incorporate residual stress into soft tissue remodelling.

The aim of this lecture is to synthesize and present current views on the rôle of residual stress in bone and soft tissues. Available models of remodelling taking into account residual stress are also presented. Particularly, the hypothesis of uniform strain distribution, due to Takamizawa and Hayashi [65, 66, 67], is critically assessed.

Part I. Hard tissues

2. Residual Stress in Osteonic Lamellae

Ascenzi and Benevenuti [2] obtained osteons from femoral shafts of human subjects aged between 19 and 31, showing no apparent skeletal defects. In turn, Ascenzi [4] obtained osteons also from the femoral shaft (human corpse, aged 35 yrs.; transverse cut: 100 μm apart). Two series of cross-sections, the first 30 and the second 100 μm thick, were prepared by grinding. The methodology of selection and dissection of osteon samples and their mechanical test-

ing was elaborated earlier by Ascenzi and his coworkers, cf. the relevant references in [2, 3, 12].

Let us now briefly describe the dissection and isolation of osteonic lamellae, cf. [2]. Each osteon sample was subjected to direct compression perpendicular to its axis and the points on its circumference, where pressure was applied were continually changed by rotation. This was done by using a glass slide on which 18×18 mm coverslip was firmly fixed with Canadian balsam. On one edge the coverslip, which was $160 \mu\text{m}$ thick, functioned as stopper during the loading. Each cylindrical osteon sample was put on the slide with its surface touching the edge of the coverslip tangentially. The osteon samples were placed in position and turned by hand, and pressure was applied by pressing a very small spatule against the side of the osteon opposite the coverslip, cf. Fig. 1. The whole process was observed under a light microscope, cf. Fig. 2.

When an osteon sample with fibre bundles in one lamella making an angle of nearly 90° with the fibre bundles in the next, is loaded perpendicular to its axis, and the direction of loading is then changed continually by rotation, arc-shaped, concentrically distributed cracks appear. They grow longer, join up and eventually become circular. The polarizing microscope reveals that the cracks involve dark lamellae, i.e. lamellae whose fibres have a marked longitudinal spiral course, while bright lamellae, i.e. lamellae whose fibres have an almost transverse spiral course, remain unaffected. Obviously, special care is to be taken to apply low or fairly low pressure-loads. With higher loads lamellae, whose fibres have almost transverse course are severely damaged too, and radical and transverse cracks appear in them.

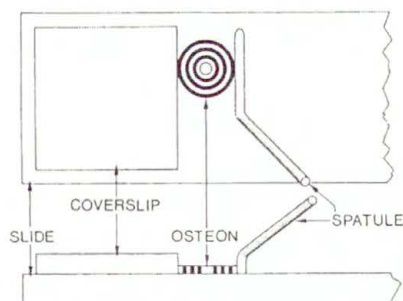


FIGURE 1. Two projection diagram showing technique to compress an alternate osteon sample perpendicular to its axis. Slide, coverslip, osteon, and spatule are clearly seen, after [4].

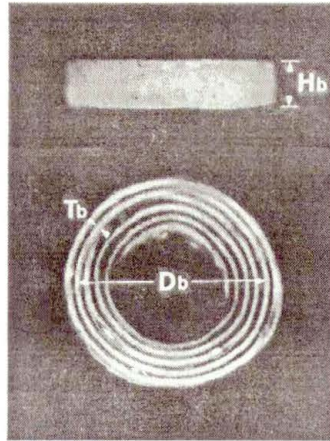


FIGURE 2. Alternate osteon containing lamellar sample: (top) view from external lateral surface ($\times 280$) showing outer height H_b of the lamella checking equal to osteon height; (bottom) sectional view ($\times 280$) showing mean diameter and thickness T_b of the lamella. Dimensions are measured by Delta Sistemi IAS 2000 image analysis system, after [4].

In alternately structured osteon samples, the circular cracks produced in lamellae with fibres having a marked longitudinal spiral course are actually deep fractures which extend to the full depth of each lamella. This allows one to isolate individual unaffected lamellae, whose fibres and crystallites have an almost transverse spiral course, using a steel needle for microscopic dissection. Dissected osteonic lamellae were next examined after immersion in a saline solution, thus resembling physiologic state. To avoid extraction artifacts, the examination of the lamellae in saline solution was reduced to a minimum. Figure 3 shows the shape of osteon lamellae, prepared by the dissection method outlined above, and possessing transversally oriented fibre bundles and crystallites.

The experimental data due to Ascenzi and Benvenuti [2] clearly show that the behaviour of isolated osteon lamellae, when they are set free in saline solution, strongly depends on their heights and diameters. For instance, lamellar samples whose height is only ca. $30 \mu\text{m}$, especially those with large diameters, show a strong tendency to twist and become strangely deformed when set free in saline solution, see Fig. 3.

Unfortunately, neither Ascenzi and Benvenuti [2] nor Ascenzi [4] investigated the influence of saline concentration on the behaviour of osteonic lamellae.

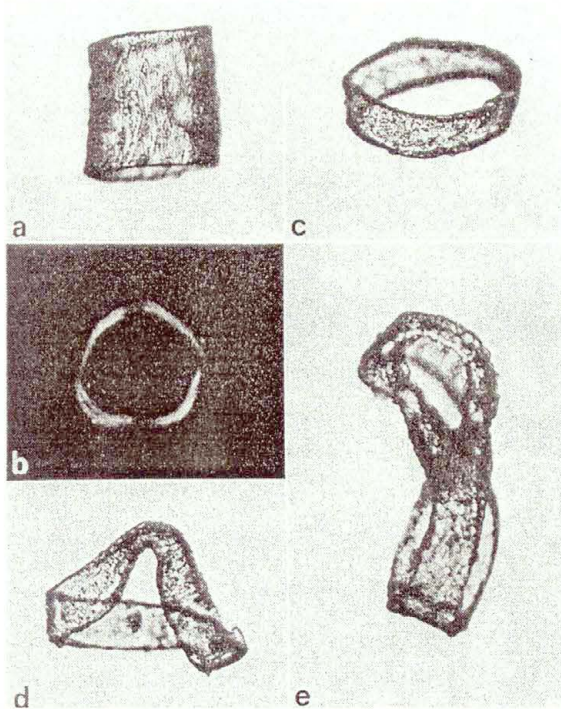


FIGURE 3. (a) Side-view of an isolated osteonic lamellar sample, ca. $100\ \mu\text{m}$ high. (b) The same sample as in (a) seen under polarizing microscope. (c) Isolated osteonic lamellar sample ca. $30\ \mu\text{m}$ high. (d) and (e) two osteonic lamellar samples ca. $30\ \mu\text{m}$ high showing clear deformations as if induced by internal stress. All the samples are fully calcified. Magnifications (a)–(c) $\times 320$, (d) $\times 750$, after [2].

Figure 4 presents a broad spectrum of osteonic lamellar samples set free in saline solution and then sectioned along a line perpendicular to its circular ends. Ascenzi and Benvenuti investigated also lamellae obtained from osteons at the initial stage of calcification. These authors claim that both types of lamellar samples, those ca. $30\ \mu\text{m}$ and those ca. $100\ \mu\text{m}$ high, are deformed in a manner similar to that of fully calcified lamellae. In our opinion such a statement is not fully justified and further investigations are needed.

Ascenzi and Benvenuti [2] investigated also decalcified lamellae. They found that such lamellae, additionally to those at the initial stage of calcification, offer evidence that the hydroxyapatite is not essential to the spiral deformation of opened lamellar samples. This is clearly depicted in Fig. 4(h–m). The lamellae shown in Fig. 4(h) and Fig. 4(i) were obtained by decalcification of the fully calcified lamellae seen in Fig. 4(a) and (b).

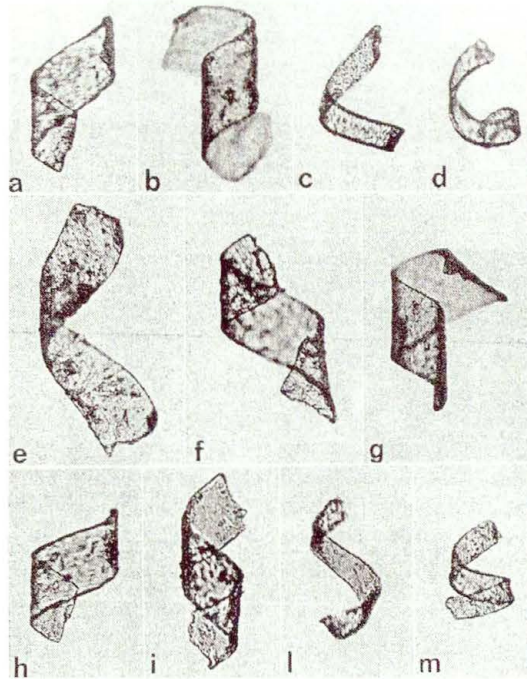


FIGURE 4. (a)–(d) Fully calcified osteonic lamellar samples after cutting. (e)–(g) Osteonic lamellar samples cut at initial stage of calcification; (h)–(m) Osteonic lamellar samples after decalcification and cutting; samples (h) and (i) are the same as (a) and (b); Magnification: (a)–(m) $\times 200$, after [2].

Ascenzi estimated residual stresses in osteonic lamellae of height $100\ \mu\text{m}$, that were cylindrical before cutting and helicoidal after cutting, cf. Fig. 3(a) and Fig. 4(b) [4]. We observe that deformation from the cylindrical to helicoidal cut lamella is geometrically nonlinear. Reported residual stress ranges up to $0.11\ \text{GPa}$. Unfortunately no details of calculation leading to estimation of residual stresses have been given.

3. Mechanical Remodelling of Bone with Residual Stress

In 1989 Seguchi [56] proposed a model of mechanical remodelling of bone with residual stress. This model is based on the *uniform stress hypothesis*. The model was further developed and applied in [1, 69, 70, 71, 72, 73].

Seguchi's idea is simple, cf. [69]. Consider two linear elastic bars with elastic moduli E_α , $\alpha = 1, 2$, which are interconnected in a statically indeterminate way, as shown in Fig. 5(a).

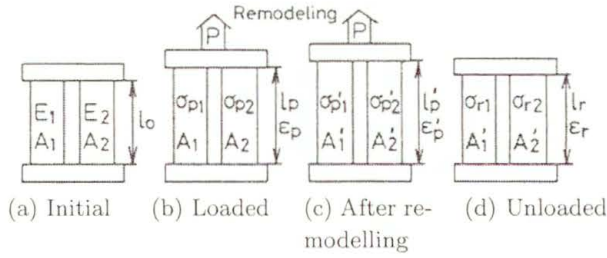


FIGURE 5. Statically indeterminate two-bar structure of a lumped parameter system, after Tanaka and Adachi [69].

Initially, these members have neither initial stress nor strains, and the relationship between stress σ_α and strain ϵ_α of each bar given by

$$\sigma_\alpha = E_\alpha \epsilon_\alpha, \quad \alpha = 1, 2 \text{ (no summation!)}. \tag{3.1}$$

The deformation of both members constrains each other, so the strain ϵ in either bar is equal to

$$\epsilon = \frac{l - l_0}{l_0}. \tag{3.2}$$

Here l denotes the deformed length and l_0 is the natural length common to both bars. When load P is applied to the structure, both bars deform elastically to length l_p resulting in strain ϵ_p and stress $\sigma_{P\alpha}$, as shown in Fig. 5(b). Then the equilibrium equation takes obviously the following form:

$$\sigma_{P1} A_1 + \sigma_{P2} A_2 = P \tag{3.3}$$

where A_α denotes the cross-sectional area of the bar α . The stress in each bar may be different, and this *difference drives remodelling*. If the *local equistress condition (uniform stress hypothesis)* is adopted as an expression of Fung's optimal performance requirement [18], a remodelling is expected to take place and decrease this stress difference until the relation

$$\sigma'_{P1} = \sigma'_{P2}, \tag{3.4}$$

becomes true under load P , cf. Fig. 5(c). This is accomplished through the change of apparent stress-strain relation toward

$$\sigma_\alpha(\epsilon) = E_\alpha(\epsilon - \epsilon_\alpha^0), \quad \alpha = 1, 2, \quad \text{(no summation!)} \tag{3.5}$$

due to the change in the cross section and/or natural length of each member. This also means that residual stresses $\sigma_{r\alpha}$ and residual strain remain in the unloaded state, as shown in Fig. 5(d) where the equilibrium equation

$$\sigma_{r1}A'_1 + \sigma_{r2}A'_2 = 0 \quad (3.6)$$

should be satisfied. This process is schematically represented as a change in the stress-strain relationship in Fig. 6.

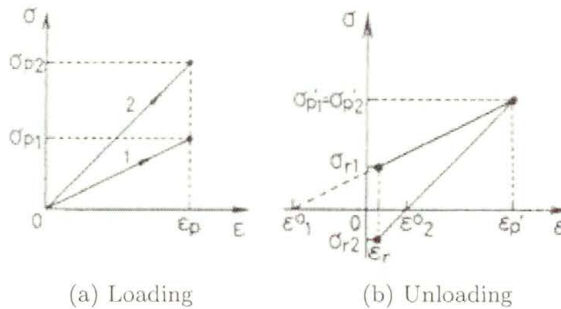


FIGURE 6. Change in stress-strain relationship due to remodelling, after [69].

This figure clearly shows the difference between the initial strains ε_α^0 (existing in the stress-free state) and residual strain ε_r (occurring when the load vanishes), the notions often confused in the biomechanical literature.

The mechanical system (3.6) is not closed. Additional equation of evolution is postulated as follows. Tanaka and Adachi [69] postulate that remodelling is essentially driven by the stress difference between the members:

$$\Delta\sigma_\alpha(t) = \sigma_\alpha(t) - \sigma_\beta(t), \quad \alpha \neq \beta; \quad \alpha, \beta = 1, 2 \quad (3.7)$$

where t denotes time.

Introducing a positive threshold value $(\Delta\sigma)^s$, the effective stress difference is defined as follows

$$\{\Delta\sigma_\alpha(t)\}^e = \text{sgn}\{\Delta\sigma_\alpha(t)\} \max\{|\Delta\sigma_\alpha(t)| - (\Delta\sigma)^s, 0\}. \quad (3.8)$$

Consequently, the volumetric change of each bar is achieved by the cross-sectional change of each member, and its rate is assumed to be given by

$$\dot{A}_\alpha(t)/A_\alpha(t) = K_\alpha\{\Delta\sigma_\alpha(t)\}^e, \quad \alpha = 1, 2, \quad (\text{no summation over } \alpha). \quad (3.9)$$

Here $\dot{A}_\alpha(t) = dA_\alpha(t)/dt$ and the parameter K_α are the positive remodelling rate of growth and atrophy in the bar α respectively. From the relation

$$\{\Delta\sigma_1(t)\}^e = -\{\Delta\sigma_2(t)\}^e \tag{3.10}$$

the sought evolution equation is given by

$$\dot{A}_2(t)/\dot{A}_1(t) = -K_2A_2(t)/K_1A_1(t). \tag{3.11}$$

Lazy zone is characterized by equating the r.h.s. of Eq.(3.9) to zero. Steady state is achieved by passing with t to infinity ($t \rightarrow \infty$).

Tanaka and Adachi [69] considered also the cross-sectional change due to remodelling during a small time interval $[t, t + \Delta t]$. Then we have

$$A_\alpha(t + \Delta t) = A_\alpha(t) + A_{y\alpha}(t), \quad \alpha = 1, 2 \tag{3.12}$$

where

$$A_{y\alpha}(t) = \dot{A}_\alpha(t)\Delta t, \quad \alpha = 1, 2. \tag{3.13}$$

Obviously, a positive value of $A_{y\alpha}(t)$ means growth and a negative value — atrophy. It was also shown that the initial strain appearing in (3.5) is given by

$$\varepsilon_\alpha^0(t + \Delta t) = \frac{A_{y\alpha}(t)\varepsilon_p + A_\alpha(t)\varepsilon_\alpha^0(t)}{A_\alpha(t + \Delta t)}, \quad (\text{no summation over } \alpha). \tag{3.14}$$

This is used to represent the change in the natural length of each bar as, cf. Fig. 7,

$$l_{0\alpha}(t + \Delta t) = [1 + \varepsilon_\alpha^0(t + \Delta t)]l_0(0), \quad \alpha = 1, 2. \tag{3.15}$$

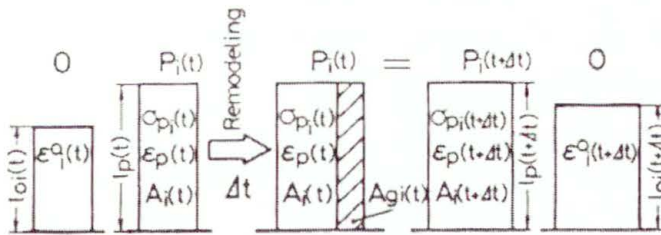


FIGURE 7. Change in natural state due to cross-sectional change by remodelling, after [69]

Tanaka and Adachi [70, p. 8] suggest the following rate equation for initial strain ε_α^0 :

$$\dot{\varepsilon}_\alpha^0 = \frac{\dot{A}_\alpha}{A_\alpha} (\varepsilon_\alpha - \varepsilon_\alpha^0), \quad \alpha = 1, 2. \quad (3.16)$$

Prior to passing to a simplified model of tibiofibula bone, consider the diaphysis of a long bone idealized as an axisymmetric, two-layered hollow cylinder shown in Fig. 8

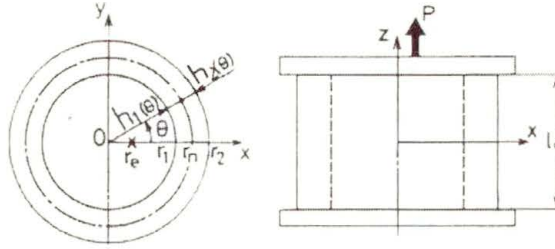


FIGURE 8. Diaphyseal model as two-layered hollow cylinder, after [69].

In Fig. 8, r_n denotes the radius of the boundary between two layers, and r_1 and r_2 are the inner and outer radii, respectively. Only the one-dimensional distribution along the circumferential direction is considered for the stress component in the z -direction. The value of stress is evaluated $r = r_n$. The thickness and elastic modulus of layer α are denoted by $h_\alpha(\theta, t)$ and E_α , respectively, cf. [69, 70]. The inner layer ($\alpha = 1$) stands for the cancellous bone whilst outer layer ($\alpha = 2$), the cortical bone so that $E_1 < E_2$. If the force acts at the point $r = r_e$ (r_e is a measure of eccentricity) and $\theta = 0$, then the equilibrium along the z -axis is written as follows

$$P = \sum_{\alpha=1}^2 \int_0^{2\pi} \sigma_\alpha(\theta) h_\alpha(\theta) r_n d\theta. \quad (3.17)$$

Similarly, we write

$$P r_e = \sum_{\alpha=1}^2 \int_0^{2\pi} \sigma_\alpha(\theta) h_\alpha(\theta) r_n^2 \cos \theta d\theta. \quad (3.18)$$

The strain $\varepsilon(\theta)$ in the z -axis direction is defined as the nominal strain by referring to the uniform natural state, cf. Eq. (3.2). The deformation is constrained by rigid plates. Hence the strain $\varepsilon(\theta)$ distribution in the x -direction

takes the form

$$\varepsilon(\theta) = \alpha + \beta x = \alpha + \beta r_n \cos \theta.$$

The rate of thickness change of each layer α due to remodelling is expressed by

$$\dot{h}_\alpha(\theta, t)/h_\alpha(\theta, t) = K_\alpha \{\Delta\sigma_\alpha(\theta, t)\}^e - C_\alpha(\theta) \{\nabla^2\sigma_\alpha(\theta, t)\}^e, \quad (3.19)$$

where $\{\nabla^2\sigma_\alpha(\theta, t)\}^e = \max\{\nabla^2|\sigma(\theta, t)| - (\nabla^2\sigma)^s, 0\}$. Here the positive threshold $(\nabla^2\sigma)^s$ is used for the lazy zone. The constants K_α and C_α can be found in [69].

Consider now this two-layered, hollow cylinder subject to a centric load ($r_e = 0$). The stress is now uniformly distributed in the circumferential direction of the θ -axis, and the first term on the r.h.s. of Eq. (3.19) drives remodelling. The initial natural state is assumed to be uniform, and remodelling is investigated under repeated loading with the period of $2\Delta T$, cf. Fig. 9(a).

The thresholds of the remodelling of the lazy zone are $(\Delta\sigma)^s = 0.1$ MPa and $(\nabla^2\sigma)^s = 0.1$ MPa, respectively and ΔT is set to unit time.

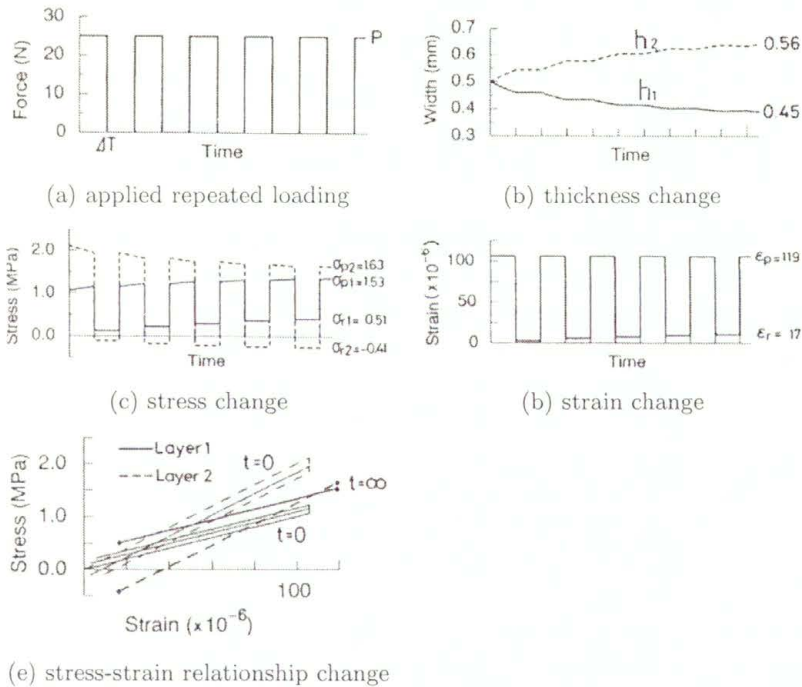


FIGURE 9. Remodelling of diaphysis model, modified after [69].

The calculated change in the thickness of each layer with time, due to remodelling, is shown in Fig. 9(b). At the time $t = 0$, the applied load of $P = 25$ N results in the stress of $\sigma_{P1} = 1.06$ MPa and $\sigma_{P2} = 2.12$ MPa in layers 1 and 2 respectively. We observe that in [70], $P = -25$ N and then $\sigma_{P1} = -1.06$ MPa and $\sigma_{P2} = -2.12$ MPa.

Remodelling is initiated by this stress difference between layers. As remodelling progresses under the external cyclic load P , layer 2 grows and decreases stress σ_{P2} . In contrast, layer 1 undergoes atrophy (resorption) and the stress σ_{P1} increases. The *difference in stresses between layers* decreases with time, cf. Fig. 9(c), (d). After some time, the difference in the residual stresses between layers is smaller than the range of the lazy zone, and remodelling does not occur during this unit time without external load. As time runs, the difference in residual stresses between layers increases. As a result of successive remodelling in both loaded and unloaded states, the process tends to the steady state without change in thickness, cf. Fig. 9(b, c and d). Figure 9(e) depicts the apparent stress-strain relationship of each layer with time.

Consider now the case of *remodelling under eccentric load*. The system investigated is the same as previously. Now the stress is distributed nonuniformly in the circumferential direction, and the second term on the r.h.s of Eq. (3.19) also becomes active upon remodelling. We assume that the repeated load is applied at the point $r_e = 0$, $\theta = 0$. Initially, the tissue is in a uniform natural state, and the stress is distributed in each layer, cf. the solid line in Fig. 10.

The change in the cross section due to remodelling is shown in Fig. 11. As can readily be seen, the remodelling results in non-uniform distribution of thickness in both layers of the model.

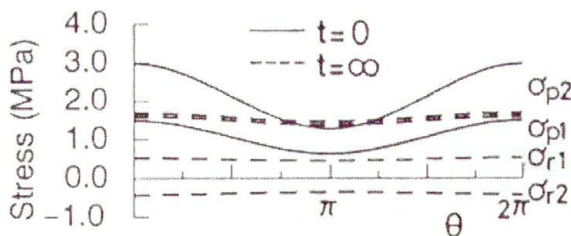


FIGURE 10. Stress distribution in diaphysis (remodelling under eccentric load), after [69].

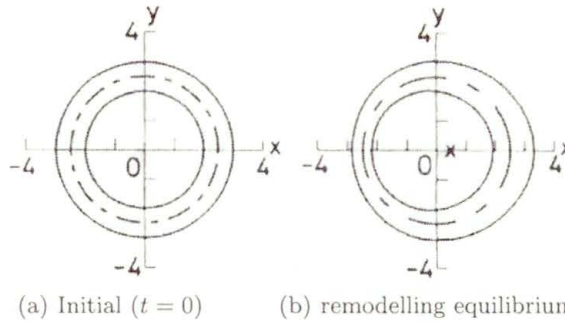


FIGURE 11. Cross section of diaphysis (remodelling under eccentric load), after [69].

First application: rabbit tibiofibula bone

The remodelling of tibiofibula bone was investigated in [69, 70, 71]. Idealized model of the tibiofibula system is presented in Fig. 12.

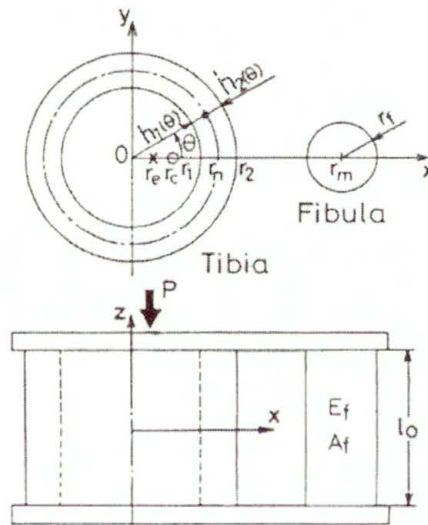


FIGURE 12. Idealized model of tibiofibula system, modified after [69].

Additionally to the previous case we have to consider the fibula, being treated as a circular solid column of radius r . The overall centroid of the tibiofibula system is at the point of r_c , indicated by the circle in Fig. 12. As previously, the load acts along the z -axis and is applied at the point of r_e and $\theta = 0$ (the cross in Fig. 12).

The equilibrium equations of the force and moment (with respect to the y -axis) are given by

$$P = \sum_{\alpha=1}^2 \int_0^{2\pi} \sigma_{\alpha}(\theta) h_{\alpha}(\theta) r_n d\theta + A_f \sigma_f, \quad (3.20)$$

$$Pr_e = \sum_{\alpha=1}^2 \int_0^{2\pi} \sigma_{\alpha}(\theta) h_{\alpha}(\theta) r_n^2 \cos \theta d\theta + A_f \sigma_f r_m, \quad (3.21)$$

where A_f denotes the cross-sectional area of the fibula.

Now the stress in the tibia is obviously influenced by the presence of the fibula; however the rate of thickness of the tibia still obeys the rule (3.19).

Let us pass to a discussion of remodelling under cyclic loading between zero and $P = -25$ N, applied at $r_e = 0.5$ mm. This corresponds approximately to a tibiofibula system under a load twice the body weight of a rabbit weighting 2.5 kg. The model parameters describing the tibia coincide with those used previously; moreover $r_f = 1$ mm and $E_f = 15.0$ GPa. We do not postulate the lazy zone to emphasize the effect of stress regulation by remodelling. The uniform natural state is again assumed as the initial state.

The initial stress distribution in the tibia under load P is shown by the solid lines in Fig. 13, depicting σ_{P1} and σ_{P2} .

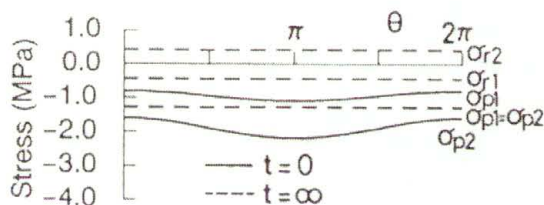


FIGURE 13. Stress distribution in tibia, after [69].

Now the magnitude of stress in the tibia becomes maximum at the site of $\theta = 0$, at which tibia faces the fibula, yielding the compressive stress (-0.89 MPa) in the fibula. The residual stresses in the tibia are shown in Fig. 13. The tensile residual stress $\sigma_f = 0.17$ MPa also remains in the fibula in the unloaded state.

The cross section of the tibia after remodelling is shown in Fig. 14.

We see that the thickness decreases at the lateral side of the tibia facing the fibula; its increase is observed at the medial site. The overall centroid of

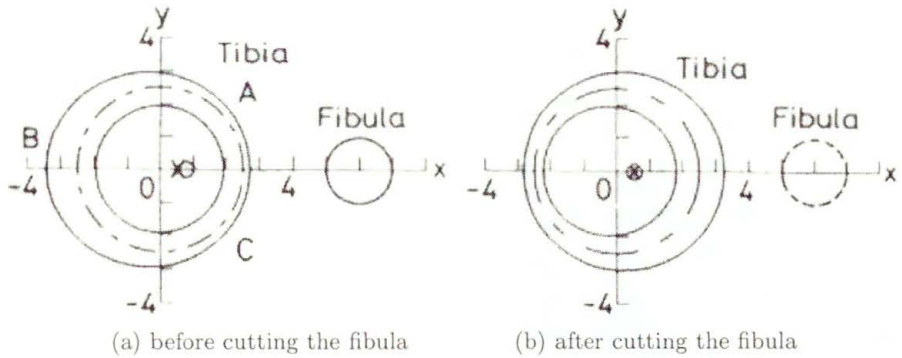


FIGURE 14. Tibiofibula system at remodelling equilibrium, after [69].

the tibiofibula system moves from the initial position at $r_c = 1.20$ mm toward the loading point $r_e = 0.5$ mm and settles at $r_c = 0.73$ mm.

It is instructive to investigate what happens after cutting the fibula and to compare the results with experimental data performed on rabbits, cf. [69, 70, 71]. Fibula cutting partially releases the residual stress found previously. The results are depicted in Figs. 14(b), 15 and 16.

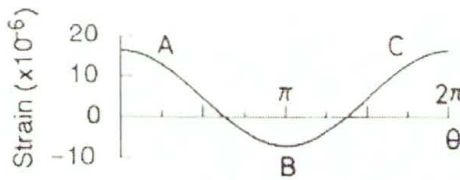


FIGURE 15. Tibia strain after cutting fibula, from [69].

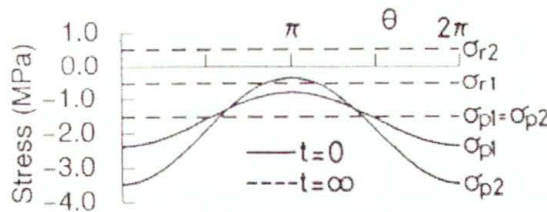


FIGURE 16. Stress distribution after cutting fibula, after Tanaka and Adachi [69].

In Fig. 16 circumferential positions labeled A, B, and C correspond to the gauge sites employed in the experiment briefly described below. The strain change qualitatively agrees with the experimental data, as shown in Fig. 17(b).

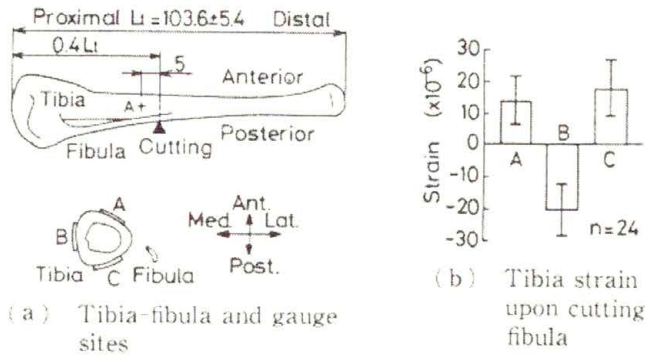


FIGURE 17. Fibula-cutting experiment in rabbit, after [69].

Upon cutting the fibula, the centroid of the tibia moves to the position $r_c = -0.39$ mm, and the stress distribution under load P becomes uniform, as shown by solid lines in Fig. 16. When the system without the fibula remains under the same loading conditions between zero and $P = -25$ N, remodelling is reactivated due to the stress distribution along the circumferential direction and between the layers. The stress achieves maximum in absolute value at the lateral site of $\theta = 0$ at the new initial time of $t = 0$. After remodelling, the cross section of the tibia changes to that shown in Fig. 14(b) at the remodelling equilibrium ($t = \infty$), and the centroid of the cross section coincides with the position of the loading point r_e .

Let us present now concisely the experimental data. Strain gauges are attached to the surface of the rabbit tibia. By cutting the fibula, the residual stress in the tibiofibula statically indeterminate system is partially released, and the strain changes were observed, cf. [69, 70, 71].

Hind limbs were excised from twelve Japanese white rabbits weighting 2.5 ± 0.1 kg (mean \pm S.D.). The tibia and fibula are cleaned of muscle attachment and the periosteum. The diaphysial surface of the tibia was scraped clean and swabbed dry, and three uniaxial waterproof strain gauges A, B and C, are bonded to the surface along the longitudinal axis using cyanoacrylate adhesive. The position of the centre of each gauge grid is marked with cross-

hairs, cf. Fig. 17(a). The tibia is immediately returned to the physiological saline bath at room temperature of 21°C. All the measurements were performed in this bath. A dummy gauge was placed in the same saline bath to compensate the drift due to change in temperature. The resolution of the measuring instrument was one microstrain, and the value of the drift was negligibly small compared to the measured values.

In the rabbit, the fibula branches from the tibia at mid-diaphysis and connects at the proximal end of the tibia, forming a statically indeterminate structure. By cutting fibula at the position marked by the solid triangle in Fig. 17(a), statical indeterminacy is partially released, and the deformation of the tibia can be measured using strain gauges. Averaged values of the strain of twelve specimens along the longitudinal direction measured using gauges A, B, and C are shown in Fig. 17(b). Positive strains were measured using gauges A and C at posterolateral and anterolateral sites whilst negative strain was observed using gauge B at the medial site. The change in strain is induced by the release of the residual stresses in the statically indeterminate structure consisting of the tibia and fibula. We conclude that the lateral side of tibia was compressed, and the medial side was stretched, and the fibula was stretched, bending the tibia in the lateral direction.

Second application: bovine coccygeal vertebrae

Adachi et al. [1] used the uniform stress hypothesis to the study of bovine coccygeal vertebrae. Experimental data concerning residual stresses were also delivered, cf. also [70, 71, 73].

We pass now to a concise presentation of the results achieved in just mentioned papers of Japanese researchers. More precisely Adachi et al. [1] investigated twelve tails of approximately two-year-old steers, immediately after slaughter. The most cranial coccygeal vertebra from each was stored at -40°C until the experiment. The vertebral specimens were freed from adhering soft tissues such as muscles, ligaments, vertebral disks, and periosteum, and kept at rest in a physiological saline bath at a fixed temperature of 20°C for more than 4 hours.

The surface of the specimen was scraped clean and swabbed dry. Two bi-axial water-proof strain gauges (SKF-20250: Kyowa Electronic Instruments Co. Ltd.) were bonded on the cortical surface using cyanoacrylate adhesive symmetrically positioned with respect to the saggittal plane between the spinous process and the transverse process on the middle plane in the

cephalocaudal direction, as indicated with crosses (R and L) in Fig. 18. The principal axes of the gauges were arranged in the cephalocaudal and circumferential directions.

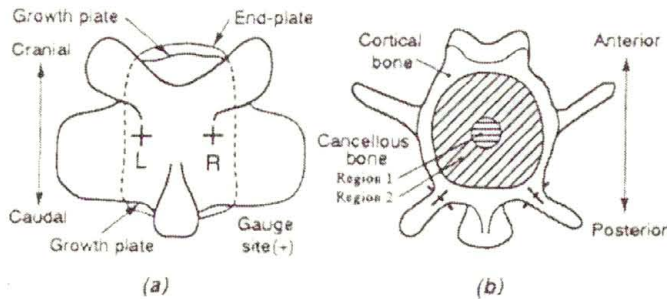


FIGURE 18. Observed strains in cutting experiment, after [1]

Adachi et al. [1] used the classical cutting method to estimate experimentally residual stress. In the case of bovine vertebrae, strain would be induced at gauges on the cortical surface, if any residual stress in the cephalocaudal and circumferential directions remained in the vertebral body. The test procedure ran as follows:

- (i) The reference state for the strain measurement was determined after the specimen with strain gauges had been maintained in the saline for 2 hours.
- (ii) Both cranial and caudal end-plates, presented in Fig. 18(a), were removed by cutting, the cranial and caudal growth plates with a hand-saw. The specimen was kept in the saline bath for more than 1 hour, and then the strain induced at the gauge was recorded.
- (iii) A circular solid region, 6 mm in diameter, the horizontally hatched *region 1* in Fig. 18(b), was removed from the central portion of transverse section of the cancellous bone using a light-duty cutter. The specimen was then kept in the saline bath again for more than 1 hour, and then the strain at the gauge was recorded.
- (iv) The remaining cancellous bone, *region 2* in Fig. 18(b), was then removed using the same rotary cutter, and the strain was recorded after the specimen had been kept in the bath for more than 1 hour.

The described cutting sequence was selected because of geometry of the vertebral body. It was assumed that one part of the cutting does not affect the other cutting sequence, which cannot be tested experimentally. On account of this assumption and assumption of small strains, one can exploit the principle of superposition for strains. The resolution of the measurement instrument (UCAM90A: Kyowa Electronic Instruments Co. Ltd.) was of single microstrain order (10^{-6}).

Let us pass to description of the strains observed by Adachi et al. [1], cf. Fig. 19.

In this figure $\Delta\varepsilon_z$ and $\Delta\varepsilon_\theta$ denote the average strains of the right and the left gauges in the cephalocaudal and circumferential directions, respectively. Data from right and left gauge sites are presumed to represent a single behaviour, since the paired analysis does not show significant differences between two gauge sites. Anyway, according to Adachi et al. [1], the total resultant strains were tensile strains: $\Delta\varepsilon_z^{\text{total}} = 64.2 \pm 50.4 \times 10^{-6}$, $\Delta\varepsilon_\theta^{\text{total}} = 40.4 \pm 38.1 \times 10^{-6}$ on average.

To perform simple theoretical analysis, the vertebral body was simplified in a manner presented in Fig. 20.

Due to rigid plate at both ends the systems presented in Fig. 20 are statically indeterminate. Regions 1 and 2 of cancellous bone and the cortical bone are referred to as members 1, 2, and 3, respectively. Obviously E_{ai}

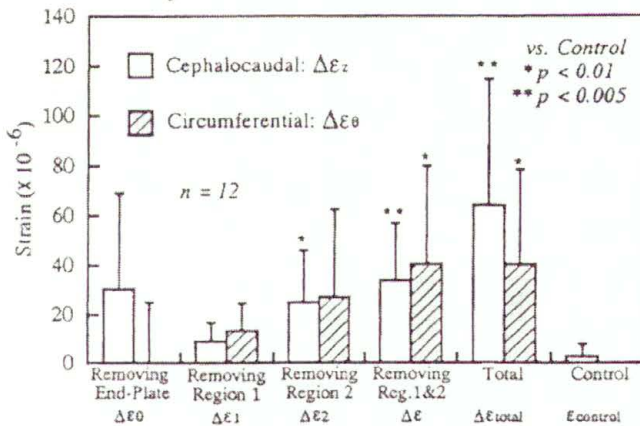


FIGURE 19. Observed strains in cutting experiment, after [1]

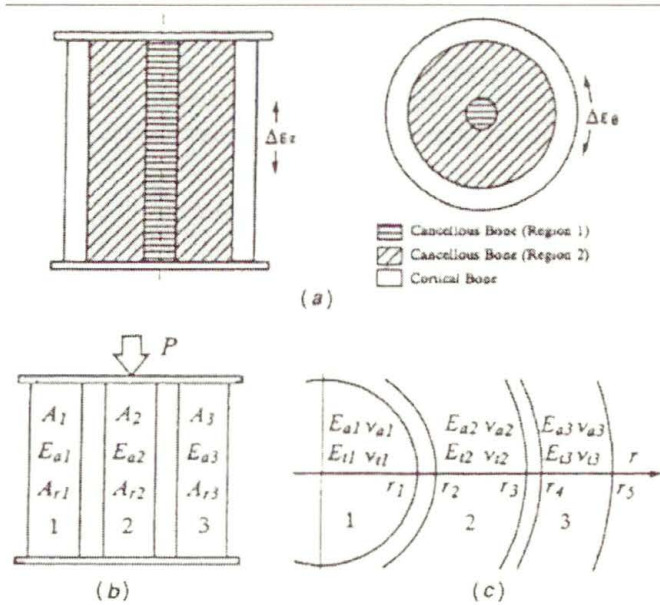


FIGURE 20. Simple model of vertebral body: (a) three-layered cylinder model of vertebra, (b) three-bar model, (c) three-layered plane strain model, after [1].

($i = 1, 2, 3$) is the Young modulus along the axis of symmetry; E_{ti} denotes the Young modulus in the transverse plane. Similar notation holds for the Poisson ratio ν_{ai} and ν_{ti} .

A three-bar model shown in Fig. 20(b) was used for the analysis in the cephalocaudal direction. Under load P acting on this three-bar system, the member stress σ_{Pi} is expressed by

$$\sigma_{Pi} = E_{ai}(\epsilon_P - \epsilon_i^0), \quad i = 1, 2, 3. \tag{3.22}$$

Here ϵ_p stands for the strain common to every bar. We have

$$\sigma_{P1}A_1 + \sigma_{P2}A_2 + \sigma_{P3}A_3 = P. \tag{3.23}$$

Now the porosity of cancellous bone is taken into account; thus the stress σ_{Pi} is different from the effective stress σ_{Pi}/ϕ_{A_i} of bone material itself. Here ϕ_{A_i} is the area fraction of bone material in the cross section.

The *uniform stress hypothesis* is expressed by

$$\frac{|\sigma_{P1}|}{\phi_{A_1}} = \frac{|\sigma_{P2}|}{\phi_{A_2}} = \frac{|\sigma_{P3}|}{\phi_{A_3}} = \sigma_z^{eq}, \tag{3.24}$$

where σ_z^{eq} is the uniform stress at the *remodelling equilibrium*. Figure 21 depicts the stress-strain relations of the bars with (different) initial strains ε_i^0 and different area fractions. For the cortical bone one may assume $\phi = 1.0$. We note that Eq. (3.24) is more general than Eq. (3.4) used for the two-bar system.

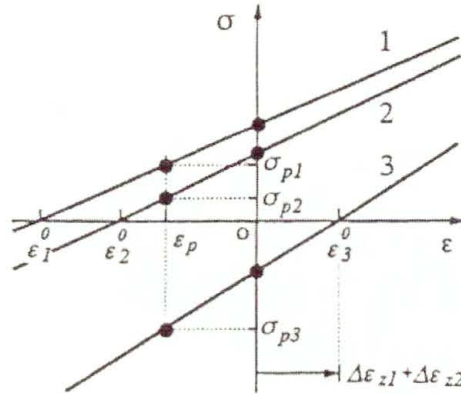


FIGURE 21. Stress-strain relations in three-bar model.

Adachi et al. [1] estimated σ_z^{eq} to equal to $\sigma_z^{\text{eq}} = 1.92 \pm 1.29$ MPa; moreover they obtained $\varepsilon_P = -54.7 \pm 38.8 \times 10^{-6}$ and $P = -178.1 \pm 121.0$ N.

For the analysis in the circumferential direction, the three-layered structure presented in Fig. 20(a) is simplified to a shrink fit model, shown in Fig. 20(c), as a plane strain problem in the (r, θ) plane at the gauge site. We observe, that the radii in natural states are different from each other in general, as $r_1 \neq r_2$ and $r_3 \neq r_4$. Just this difference brings the contact pressures at the interfaces between the adjacent layers and the residual stress in each of the cylinders in the circumferential direction into the model shown in Fig. 20(a). The uniform stress in radial direction σ_r^{eq} at the interface between cylinders 1–2 was estimated as $\sigma_r^{\text{eq}} = 0.63 \pm 0.62$ MPa. Of the same order is the circumferential uniform stress $\sigma_\theta^{\text{eq}} = 0.67 \pm 0.57$ MPa, cf. [1].

To conclude this section it is worth noting that the uniform stress hypothesis enables to take into account residual stress in bone structures treated as indeterminate system. Further developments are needed to use to, say to three-dimensional system. Also, nothing can be said about evolution of bone microstructure.

A comment on residual stresses at the stem-cement interface

Such a problem is of practical value in orthopaedic biomechanics. Nuño and Avanzolini [44] performed a finite element analysis pertaining to influence of residual stresses at the stem-cement interface of cemented hip implants. The geometry of the idealized cylindrical hip stem inserted into bone is shown in Fig. 22.

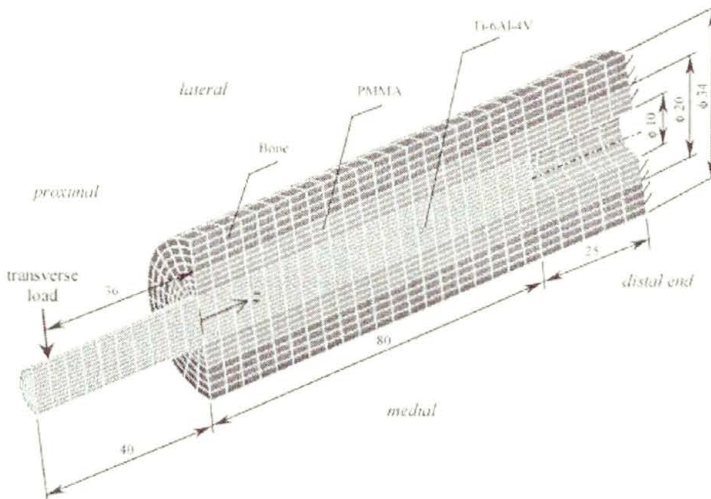


FIGURE 22. Three-dimensional finite element mesh of the cemented hip stem analyzed. All dimensions in mm, after Nuño and Avanzolini [44].

All the materials were assumed to be linear elastic, isotropic and homogeneous. The Ti-6Al-4V stem had Young's modulus $E = 110\,000$ MPa and Poisson's ratio $\nu = 0.3$; the PMMA cement mantle had $E = 2700$ MPa and $\nu = 0.35$; the cortical bone had $E = 15\,500$ MPa and $\nu = 0.28$. The distal ends of the cement mantle and the bone were completely fixed. The cement-bone interface was assumed rigidly fixed, while the stem-cement interface consisted of 294 nonlinear contact elements *Contact52*, 3D node-to-node elements, using Coulomb friction behaviour allowing for sticking and sliding. A coefficient of friction $\mu = 0.2$ was assumed (at the stem-cement interface).

The compressive residual radial stress due to cement curing at the stem-cement interface was simulated by a press-fit effect: an interference of $5\ \mu\text{m}$ was assigned to the contact elements corresponding to radial residual stress of approximately 2.4 MPa. We observe that residual stress can likewise be generated by thermal expansion.

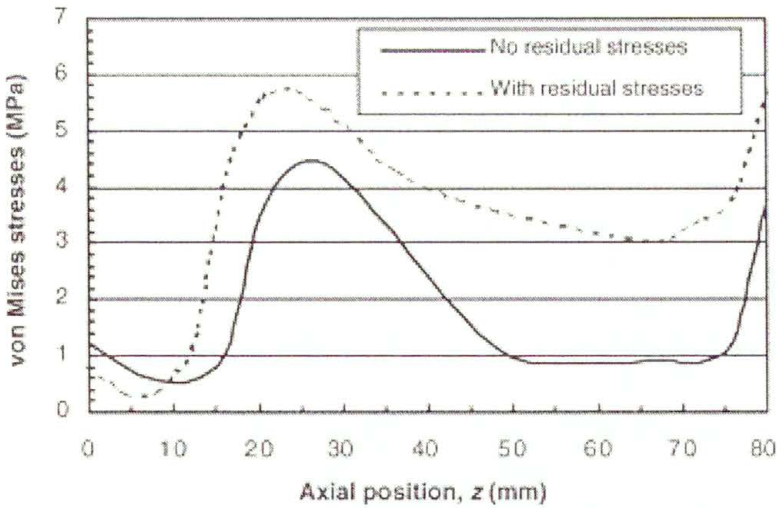


FIGURE 23. von Mises stress in the cement mantle at the interface on the lateral side without and with residual stresses, versus the axial coordinate z , after [44].

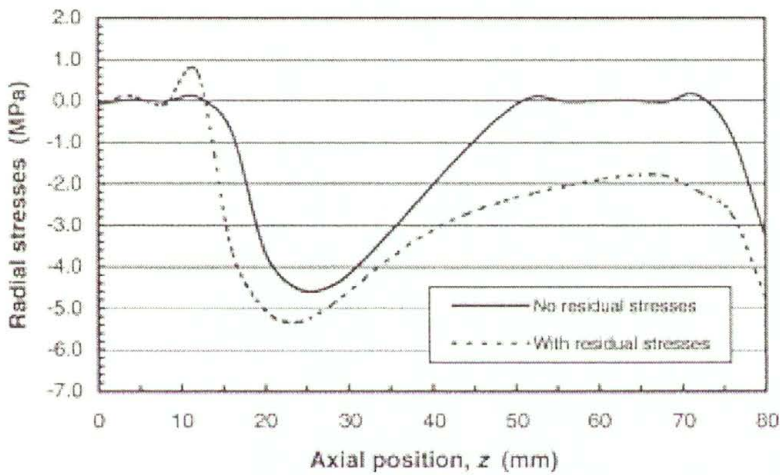


FIGURE 24. Radial stress in the cement mantle at the interface on the lateral side for without and with residual radial stress versus the axial coordinate z ; after [44].

Significant influence of residual stress is clearly shown in Fig. 23 and Fig. 24.

The analysis performed by Nuño and Avanzolini [44] is simplified since the issue of bone cement polymerization has not been considered, cf. [60].

Part II. Soft tissues

In this part we intend to synthesize main developments pertaining to existence of residual stress in soft tissues and its influence on adaptation. As we already know, residual stress was primarily shown to exist in bone and then in tissues like bovine and porcine aortas and the left ventricle of rabbit (cf. [18, 52]). It is also known to exist in living tree. More precisely during the growth, an internal stress is generated in cambium zone of a tree and is named growth stress, cf. Okuyama and Yamamoto [48].

4. Aorta and Arteries

According to Rachev and Greenwald [55] it has been known for at least 40 years, since the Ph.D. thesis by Bergel [5], that when a ring segment is cut from an artery and an axial cut is made in the ring, it uncoils like a watch spring. In the pioneering paper by Vaishnav and Vossoughi [76] 3 bovine and 9 porcine aortas were examined; see also the paper by these authors [75]. In a typical experiment, the segment of the aorta extending from just below the aortic arch to the distal end of the abdominal aorta was freed of the loose tissue on the adventitia and gently laid down in its natural configuration. We recall that the blood vessel wall consists of three layers: the intima, media, and adventitia, cf. [6], Fung [21], Humphrey [33]. The intima is the innermost layer and contains endothelial cells. The media is the middle layer and contains the smooth muscle cells. The adventitial layer is the outermost layer and contains collagen fibres and ground substances, and some fibroblasts, macrophages, blood vessels (vasa vasorum), myelinated nerves, and nonmyelinated nerves.

We return now to the paper by Vaishnav and Vossoughi [76]. Using a sharp razor blade, transverse cuts approximately 3 to 4 mm apart were made along the entire length of aorta so as to yield a large number of almost circular rings (in fact, they were oval). From 20 to 46 rings were obtained from each aorta, with a total of 286 rings. The intact vessels as well as the rings were kept submerged or bathed in physiological saline at room temperature (from 20 to 23°). Dorsal radial cuts were made through the thickness of each ring, which opened into a horseshoe shape upon being cut. Groups of rings were photographed, along with a millimeter scale, before and after being subjected to radial cut. The sets of rings and their open configurations were labelled

for reference. Figures 25 and 26 show a set of 9 rings from a bovine aorta before and after being cut.

The annular sections were oval in shape with the largest and the smallest midwall diameters (a and b respectively in Fig. 27) not differing by more than 25 percent.

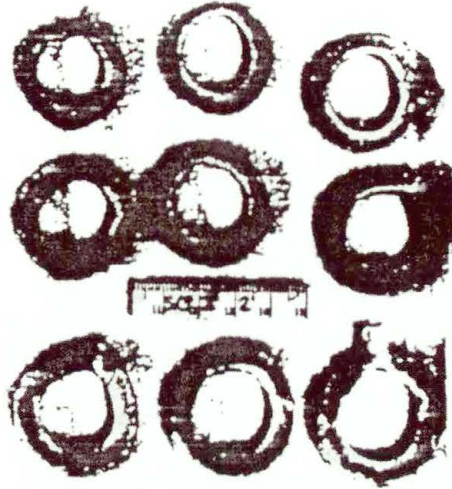


FIGURE 25. Transverse annular sections from an aortic segment. The small division on the scale represents one mm, after [76]



FIGURE 26. The open configuration obtained by radial sectioning of the transverse annular sections in Fig. 25, after [76]

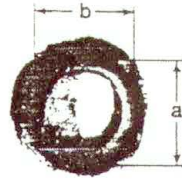


FIGURE 27. A typical transverse annular section of an aortic segment. a and b are the maximum and minimum midwall diameters of the section, generally in orthogonal directions, after [76].

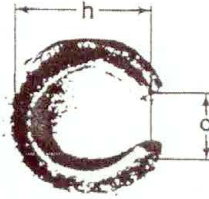


FIGURE 28. A typical transverse annular section after radial sectioning, after [76]

A mean radius for each ring was calculated as follows: $R_0 = (1/4)(a + b)$. The opened up horseshoe shapes of the rings were approximated as arcs (see Fig. 28) with their mean midwall radii R calculated according to the formula: $R = (1/8)(c^2/h + 4h)$.

Assuming that the radial lines, straight in the closed configuration remained straight and normal to the midwall curve after transition to the cut-open configuration, the circumferential engineering strain ε_θ at a radial distance r from the midwall in the closed configuration relative to the open configuration can be calculated as follows:

$$\varepsilon_\theta = r \left(\frac{1}{R_0} - \frac{1}{R} \right), \quad (4.1)$$

It was further assumed that the midwall “fibre” is strain-free. The maximum positive and negative strains will occur at $r = +t/2$ (adventitial surface) and $r = -t/2$ (intimal surface), respectively, and have a maximum magnitude

$$|\varepsilon_\theta|_{\max} = \frac{t}{2} \left(\frac{1}{R_0} - \frac{1}{R} \right). \quad (4.2)$$

Here t denotes the mean wall thickness and we preserve the notation used in [76].

Assuming that the open configuration is stress-free (now we know that such an assumption is not true), the stresses in the closed configuration at a radial distance r from the midwall curve can be estimated from a uniaxial stress-strain curve for a circumferential strip. Then, the magnitude of the maximum tensile and compressive stresses in the closed ring are calculated as follows:

$$|\sigma_\theta|_{\max} = \frac{Et}{2} \left(\frac{1}{R_0} - \frac{1}{R} \right), \quad (4.3)$$

with the intimal side being in compression and the adventitial side in tension. Here E denotes the Young modulus.

According to [76], the maximum magnitudes of the circumferential engineering strains through the wall thickness vary from 0.044 to 0.124, and the corresponding stresses vary from 44 to 124 G/cm² ($G \approx 9.81 \times 10^{-3}$ N), where an approximate value of $E = 1000$ G/cm² has been used (Vaishnav and Vossoughi write g/cm² instead of G/cm²). Furthermore, these authors estimated the maximum residual stress amounting to approximately 14 to 17 percent of the in vivo circumferential engineering stress.

The aortic wall, similarly to other vessel walls, is a layered material, hence it's inhomogeneous. The early procedure of estimation of residual stresses, outlined above, is typical for materials homogeneous through the thickness. Consider now the case when the intima is separated from the outer segment, cf. Fig. 29.

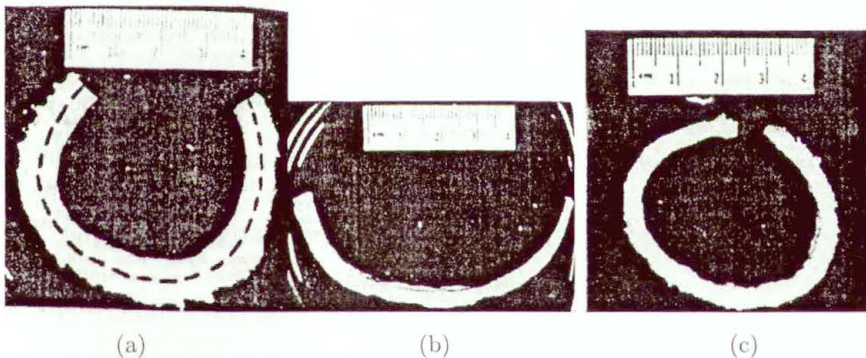


FIGURE 29. Bovine aortic ring after cutting (a) and separation of the intima (b,c) from the outer segment, after [78]

The dashed line in Fig. 29 is the line along which separation into the inner and outer layer was performed. Figure 29 clearly shows that the segment containing the intimal layer opened up significantly more than the outer

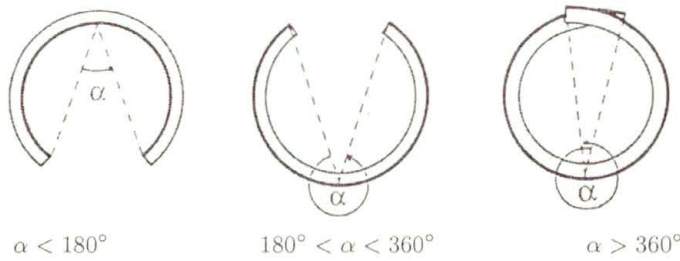


FIGURE 30. Definition of the term “opening angle”; sector represents circumferential cross section of a blood vessel at zero-stress state. Angle subtended between 2 lines originating from midpoint to tips of inner wall is the opening angle, after [20]

segment containing adventitial layer. This indicates that more residual strain was inherent to the intimal layer than that measured using Fig. 29(a)—before separation. According to Vossoughi et al. [78], the value of the intimal residual strain is approximately twice of that obtained using only one cut to the aortic ring. Unfortunately, no specific value was given. Also, it is not clear along which line the second cut was performed.

Greenwald et al. [23] showed that residual strains are not homogeneously distributed through the arterial wall. More precisely, a two-component representation of the vessel wall was assumed (the authors use the term “two-layer representation”). The two layers are not necessarily intended to represent media and adventitia. The authors assume that the residual strains present in a particular component of the wall may be quantified by eliminating the mechanical effects of the other components. The major structural components of the artery wall were removed chemically or thermally in one sets of experiments (aortas from nine male Sprague Dawley rats), and eliminated mechanically in another (bovine carotid arteries from 12 animals). Residual strains in the artery wall were found to be concentrated in the inner layers, which contain more elastin than the other layers.

Valenta et al. [77] provided experimental data on the influence of adventitia of opening angle. The concept of opening angle is illustrated in Fig. 30.

These authors performed experimental investigations using 21 specimens of the human aorta and coronary artery. The average age of subjects of both sexes was (63.6 ± 8.4) . Arterial rings of 30–80 mm in height were excised from the ascending and descending aorta, the vertex and the end of the aortic arch, between the diaphragm and above the bifurcation, and also from the right coronary artery.

Two approaches were used. In the first one the adventitial layer was mechanically removed (the membrana elastica was left undamaged). In the second approach the adventitial layer was left intact. Some of the results achieved are presented in Figs. 31–33.

Matsumoto et al. [41] performed a refined analysis aiming at the determination of residual stresses in a so-called lamellar unit of the aortic media. We recall that aortic media is made of concentric layers whose unit is just the lamellar unit, a pair of elastic lamina (EL) and a smooth muscle-rich layer (SML), cf. Humphrey [33]. Elastic modulus of elastin is about 0.6 MPa (see [18]) whilst that of the smooth muscle is of the order of 0.01 MPa in the relaxed state. Thus we see that EL is much stiffer than the SML.

If the stress-strain relationships describing the EL and SML are different, residual stresses between the two layers should also be different. Indeed, if the circumferential stress in the *in vivo* condition is the same between the soft and stiff layers, compressive residual stress will arise in the stiff layer and tensile in the soft layer, cf. Fig. 34.

Such residual stress is not fully released by radial cutting; however this stress is released in the area close to the cut surface, causing “hills and valleys” (as Matsumoto et al. write) on the surface due to compressive and tensile stresses, respectively. In the mechanical literature one uses the expression “wrinkles” and not “hills and valleys”.

To check the hypothesis that wrinkles arise on the cut surface, Matsumoto et al. [41] developed a scanning microindentation tester (SMIT), a scaled-up version of an atomic force microscope (AFM), and measured the surface topography and stiffness distribution of the cut surface of the porcine thoracic aortas. Residual stress and strain in the lamellar unit was also estimated. To this end FEM was used.

The residual stress was estimated to be (-70 kPa) for the EL and 20 kPa for the SML. These values are relatively large. Indeed, the macroscopic circumferential residual stress reported in the literature is in the range 1–10 kPa whilst the physiological stress is about 300 kPa for the rat aortas, cf. the relevant references cited in Matsumoto and Hayashi [42] and [41]. It seems that the values obtained can be viewed as an upper bound.

Let us present now the main results obtained by Fung and his coworkers, and pertaining to estimation of residual stresses and strains in the aortas and arteries.

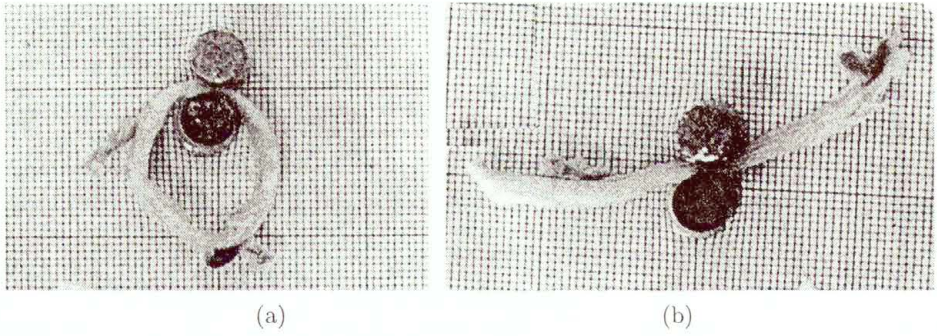


FIGURE 31. (a) The aortic ring (media and adventitia) of a 61-year old man; The ring was excised at the place of passage through the diaphragm. (b) The state observed 25 min. after radial cut. Note that the opening angle is greater than 180° , after [77]

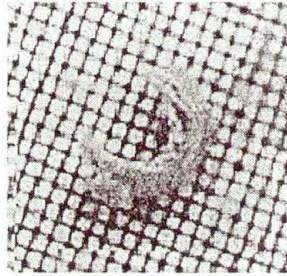


FIGURE 32. The ring of the coronary artery of 83-year old woman. The state observed 25 min. after radial cut; the opening angle is equal approximately to 180° , after [77]

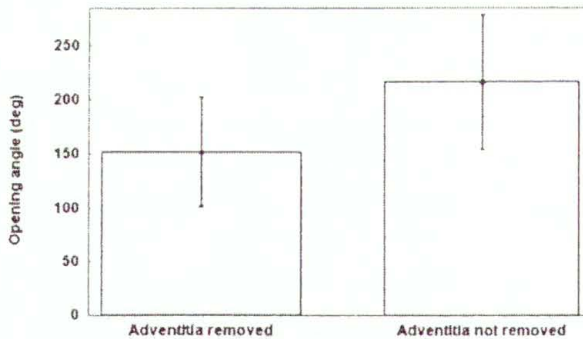


FIGURE 33. The comparison of the opening angle of specimens with removed and intact adventitia (average value \pm S.D.), after [77]

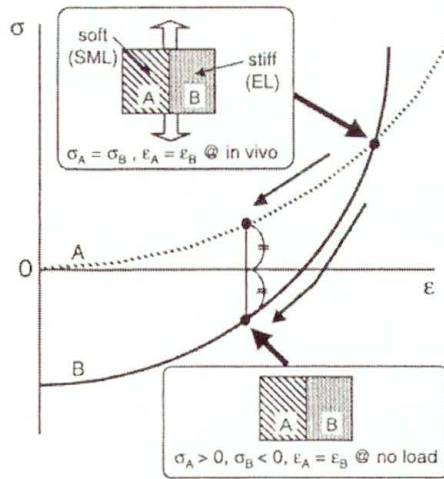


FIGURE 34. Residual stress caused by material heterogeneity; If the tensile stresses in the layers A and B are equal in a loaded state, the unloaded material has tensile stress in the soft layer (A) and compressive stress in the stiff layer (B). In the no-load state the sum of the forces in the layers (A) and (B) becomes zero, after [41].

It is commonly assumed that the artery is a cylindrical tube, whose wall material is cylindrically orthotropic, cf. [9, 10]. Assuming also that the material the tube is made of is homogeneous after the removal of residual stress from the unloaded state, the vessel wall should become a sector of constant curvature and thickness. As we already know, the last assumption is not true since the arterial wall is inhomogeneous through the thickness. Eventually, one could consider slices of, say, media without intima and adventitia. Chuong and Fung [9, 10] introduced the *effective radii* for the stress-free reference state from the noncircular opened-up configuration taken from experiments.

Figure 35 shows the idealized vessel wall configuration at various states. The stress-free reference state is called state 0, the unloaded state is state 1, and the subsequent loaded states are states 2, 3, ..., N . With cylindrical polar coordinates, a material point is denoted as (r, θ, z) in the states 1, 2, 3, ..., N . The subscripts i and e denote the internal and external wall radii at various states. Θ_0 represents half of the angle of the arterial wall at the stress-free state 0.

The angle Θ_0 and the internal and external wall radii state 0 and 1 can be determined from the direct measurements of fibre lengths on both surfaces

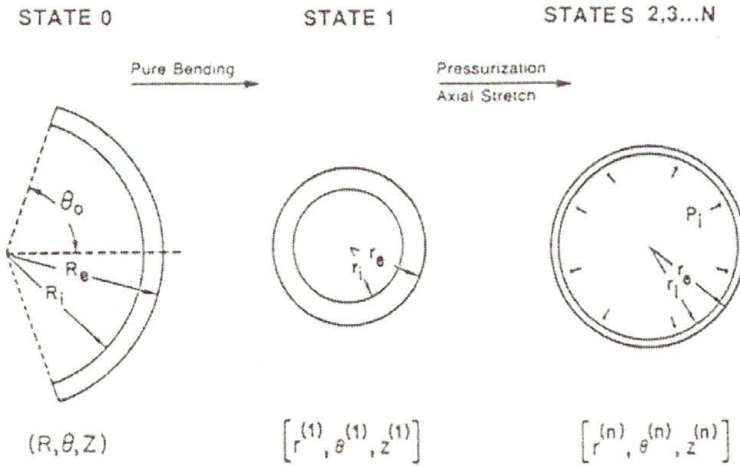


FIGURE 35. The cross-section representation of an artery at the stress-free reference state 0, the unloaded state 1, and subsequent loaded states under transmural pressure and axial force, after [9]

taken from the photos of the open-up specimen. For state 1 we have

$$2\pi r_i = l_i, \quad 2\pi r_e = l_\alpha \tag{4.4}$$

for the internal and external surfaces, respectively, where l denotes the measured fibre length. For state 0, we write

$$2\Theta_0 R_i = L_i, \quad 2\Theta_0 R_e = L_e \tag{4.5}$$

for the inner and outer walls where L denotes the fibre length measurements at this state. The determination of r_i and r_e for state 1 is straightforward. However, another equation is needed to solve for the three unknowns Θ_0 , R_i and R_e in Eq.(4.5). Such an equation is provided by the incompressibility condition of the vessel wall:

$$\Theta_0(R_e^2 - R_i^2) = \pi \lambda_z (r_e^2 - r_i^2) \tag{4.6}$$

where λ_z is the axial stretch ratio and is to be measured directly. By solving Eqs.(4.5) and (4.6), the geometric description of state 0 is determined in terms of the effective values.

The deformation of a thick-walled artery under transmural pressure and axial tethering is described by

$$r = r(R), \quad \theta = (\pi/\Theta_0)\Theta, \quad z = z(Z) \tag{4.7}$$

for the transformation of the radial, circumferential and longitudinal coordinates, respectively. The corresponding principal stretch ratios are given by

$$\lambda_r = \frac{\partial r}{\partial R}, \quad \lambda_\theta = \frac{\pi}{\Theta_0} \frac{r}{R}, \quad \lambda_z = \frac{\partial z}{\partial Z}. \quad (4.8)$$

Green's strains E_Θ , E_Z and E_r in the circumferential, longitudinal and radial directions, respectively, are related to the principal stretch ratios of Eq. (4.8) by

$$E_i = \frac{1}{2}(\lambda_i^2 - 1), \quad i = r, \theta, z. \quad (4.9)$$

The arterial wall material is assumed to be characterized by an exponential strain energy function:

$$\rho_0 W = \frac{c}{2} \exp W_1 \quad (4.10)$$

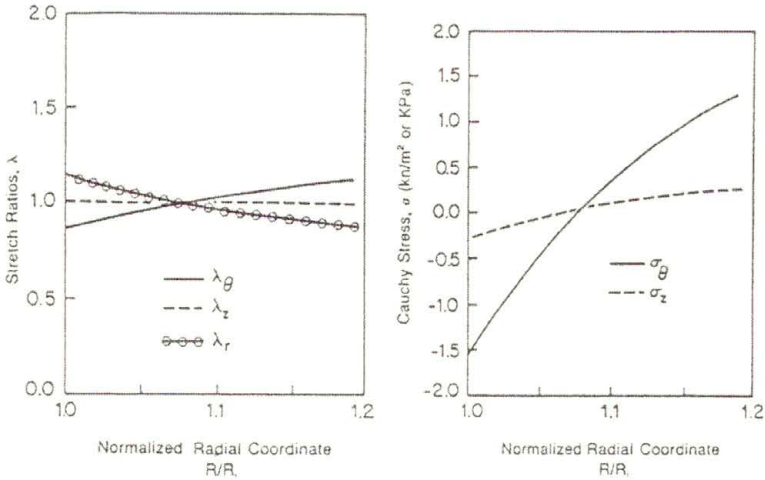
where

$$W_1 = b_1 E_\theta^2 + b_2 E_z^2 + b_3 E_r^2 + 2b_4 E_\theta E_z + 2b_5 E_z E_r + 2b_6 E_r E_\theta. \quad (4.11)$$

Here c , b_1 , b_2 , \dots , b_6 are material moduli. The wall material is assumed to be incompressible. This constraint is added to the strain energy function through a Lagrangian multiplier, cf. Part III of our lectures.

Chuong and Fung [9, 10] performed calculation for rabbit thoracic artery for the case where the measured geometric values are: $l_i = 8.75$ mm, $l_e = 12.5$ mm, $L_i = 9.75$ mm, $L_e = 11.25$ mm. Then, solving Eqs. (4.5) and (4.5), with the assumption of $\lambda_z = 1$, we obtain $R_e = 4.52$ mm, $R_i = 3.92$ mm, and $\Theta_0 = 71.4^\circ$ as the effective external, internal radii and the effective angle for the reference state 0. The material coefficients are given by: $c = 22.40$ kPa, $b_1 = 1.0672$, $b_2 = 0.4775$, $b_3 = 0.0499$, $b_4 = 0.093$, $b_5 = 0.0585$, $b_6 = 0.0042$.

Figure 36(a) presents the residual strains in the arterial wall when the vessel is unloaded. The strains are expressed in terms of principal stretch ratios. It is seen that fibres at the inner wall are shortened, while those at the outer wall are elongated. Figure 36(b) presents the distribution of the residual stresses at the unloaded state. In the circumferential direction, the inner wall has a compressive residual stress of 1.5 kPa; the outer wall has a tensile residual stress of 1.3 kPa. These are small numbers compared with stresses at loaded states shown in Fig. 37. However, their effects are significant. More precisely, Fig. 37 shows the distribution of principal stretch ratios and principal stresses of the vessel wall at $p_i = 120$ mm Hg (~ 16.0 kPa)



(a) Distributions of principal stretch ratios $\lambda_\theta, \lambda_z, \lambda_r$ (b) Distributions of residual stresses σ_θ, σ_z

FIGURE 36. Residual strains and stresses in the wall of an unloaded thoracic artery, after [9]

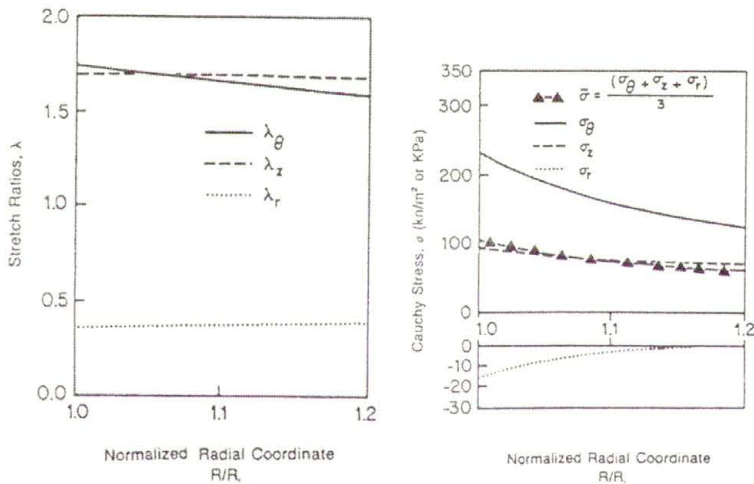


FIGURE 37. Strain and stress distributions in the wall of a rabbit thoracic artery at $p_i = 120$ mm Hg (~ 16.0 kPa) and $\lambda_z = 1.691$, after [9]

and axial stretch ratio $\lambda_z = 1.691$. The circumferential stress at the inner wall is found to be 1.42 times larger than the average value across the vessel wall. It is worth noting that in an earlier work [8], the same authors found that under the hypothesis that the unloaded tube is stress-free, the circumferential stress at the inner wall was 6.5 times larger than the average value across the vessel wall (the internal pressure is the same as previously: $p_i = 120$ mm Hg). We conclude that the removal of the hypothesis that unloaded state is stress-free has the effect of reducing the stress concentration factor from 6.5 to 1.42.

Liu and Fung [39] studied the opening angle of short segments of aorta along the aortic tree of Sprague Dawley rat, cf. Figs. 38 and 39. According to these authors, for a short segment of aorta it may be sufficient to make one longitudinal cut to assess whether after one cut the segment is in a stress-free state, cf. also Rachev and Greenwald [55].

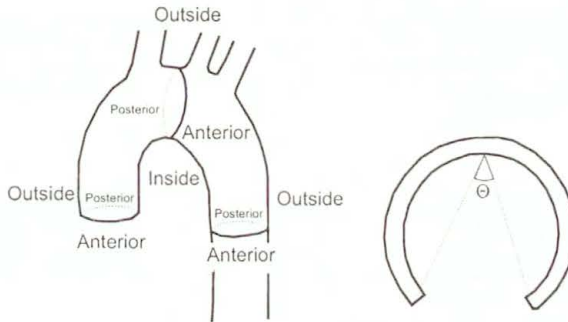


FIGURE 38. Left: Nomenclature for sites: “outerior”, “posterior”, “inside”, and “outside”. Right: Definition of the opening section angle Θ , after [39].

Fung and Liu [19] and Liu and Fung [40] reported that residual stresses in the rat aortic wall, represented by the opening angle, changed rapidly in response to the induction of hypertension. When they generated hypertension by constricting the abdominal aorta, they found a marked increase in the opening angle, from 171° to 214° in 4 days after constriction, followed by gradual decrease to an asymptotic value of 126° in 40 days in the ascending aorta. Hypertension was created in 57 Sprague-Draw rat by banding abdominal aorta with a metal clip 0.51 mm wide and 6.61 mm in length.

Fung and Liu [20] also observed similar and faster change in the opening angle in rat pulmonary arteries subjected to hypoxic hypertension: the angle increased from 294° to 385° in 12 h and then decreased gradually to 193° in 240 h. By comparing the changes in opening angle with histological obser-

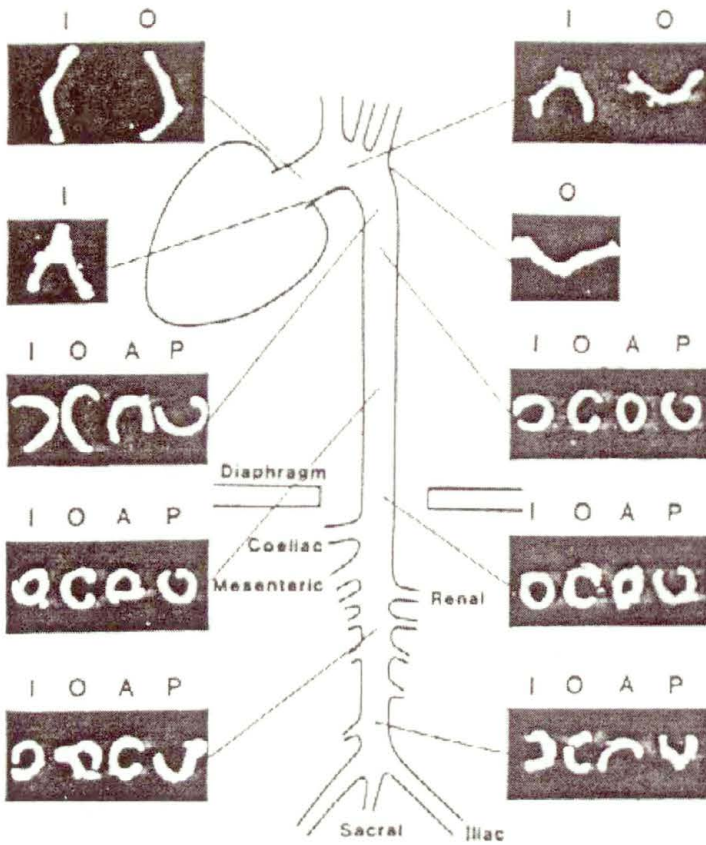


FIGURE 39. Photographs of the zero-stress configuration of aorta along the aortic tree (of rat). The symbols A, P, I, O stand for anterior, posterior, inside, and outside, respectively (see Fig. 38), after [39]

vation, they explained the opening angle by the nonuniform remodelling of artery wall.

Chuong and Fung [9] proposed a method of direct measurements of residual strains in aorta. The method consist in sprinkling small microdots of water-insoluble ink onto the surface of the transverse sections of aortic segments. It seems that nowadays one could use laser or speckle methods.

A natural question is: what is histological change associated with hypertension?, cf. Matsumoto and Hayashi [42]. To answer, at least partially, this question, consider Fig. 40. The figure shows micrographs of the aortic sections of control, hypertensive, and severely hypertensive rats. It is obvious that the total wall thickness was increased by the elevation in blood pressure.

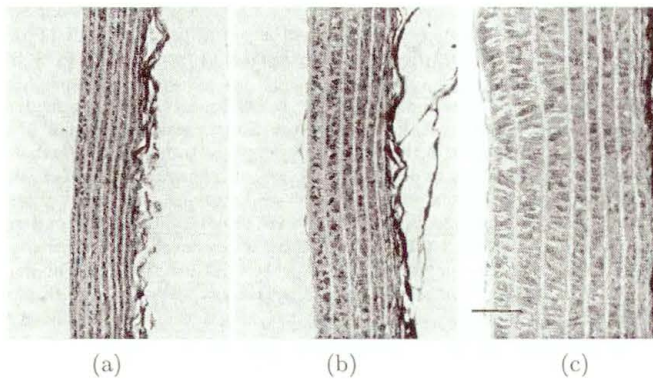


FIGURE 40. Micrographs of the thoracic aorta in three operated rats, fixed under in vivo loading condition and stained with Azan (a) Normotensive rat ($P_{\text{sys}} = 145$ mmHg), (b) hypertensive rat ($P_{\text{sys}} = 200$ mmHg). (c) Severely hypertensive rat ($P_{\text{sys}} = 240$ mmHg). Sections are parallel to the longitudinal axis of the vessel; intimal surfaces face left. Length marker ($50 \mu\text{m}$) in (c) applies to all parts of the figure, after [42]

The lamellar units had almost the same thickness throughout the wall thickness in the normotensive rat (Fig. 40(a)), whilst in the severely hypertensive rat (Fig. 40(c)) the units were much thicker near the inner surface than near the outer surface.

The thickening of the lamellar units was associated mainly with the increase of ground substance and partly with the hypertrophy of smooth muscle cells. It may thus be said that hypertension caused the wall thickening, especially in the subintimal region.

Han et al. [25] studied the opening angle of the autogenous vein grafts of seventeen mongrel dogs, 15–21 kg in body weight (30 canine grafts). Canine femoral veins were grafted to femoral arteries in the end-to-end anastomosis fashion. The results show that the opening angles (mean \pm S.D.) are $63.0 \pm 30.6^\circ$ for normal femoral veins, and $-0.4 \pm 4.6^\circ$, $6.1 \pm 19.4^\circ$, $25.4 \pm 20.1^\circ$, and $47.8 \pm 11.4^\circ$ for vein grafts at 1 day, 1 week, 4 and 14 weeks post surgery, respectively, cf. Fig. 41. The postsurgical changes in opening angle reveal nonuniform transmural tissue remodelling in the vascular wall.

Rachev et al. [53] developed a mathematical model which accounts for both the geometrical and mechanical remodelling of arteries in response to induced hypertensions, cf. also the lecture by A. Rachev in this volume. An essential point is to incorporate the remodelling rate equations. The problem was reduced to 4 evolution equations for four growth parameters.

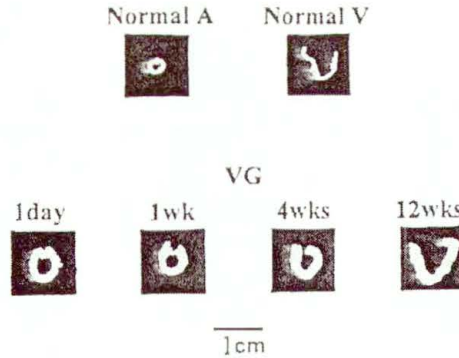


FIGURE 41. Photographs of typical configuration of zero-stress states of the short segments of a normal femoral artery (Normal A) a vein (Normal V), vein grafts (VG) at 1 day, 1 week, 4 weeks and 12 weeks post surgery, after [25]

Taber [62] proposed a biomechanical growth law for arteries and examined the behavior of a thick-walled tube model of aorta under various conditions during development and maturity.

Taber and Humphrey [64] studied the effect of heterogeneous material properties on growth-induced residual stress in arteries (mainly rat aorta and bovine carotid artery) and the utility of using opening angles to characterize this residual stress.

Uniform circumferential stress assumption was adopted by Ogden and Schulze-Bauer [47]. These authors obtained the sign of residual stresses opposite to those reported by Chuong and Fung [10] and Takamizawa and Hayashi [66].

Delfino et al. [14] developed a model of the carotid artery bifurcation for studying the wall stress field. The proposed model includes thick wall with varying thickness, nonlinear elastic property (isotropy) and the zero stress state.

5. Heart

The opening angle concept has also been used to characterization of residual stresses and strain in the left ventricle; cf. [49, 51, 63] and the references therein.

Takamizawa and Matsuda [68] proposed a mathematically sophisticated model of soft tissues with residual stresses. The hypothesis of uniform strain

distribution (through the wall thickness) was employed. As a particular case a spherical model of the left ventricle was studied. The uniform strain hypothesis was advanced by Takamizawa and Hayashi [65], cf. also Takamizawa and Hayashi [66, 67]. To put it briefly in the uniform strain hypothesis “strain” means the strain referred to a stress-free configuration. The hypothesis implies that the circumferential stretch ratio, $\lambda_{\Theta}^{(p)}$, is independent of the radius $R^{(p)}$; superscript (p) indicates the standard physiological state.

Summerour et al. [61] showed that opening angles (in rats) were significantly higher in ischaemic hearts than in sham-operated or strain-softened hearts, suggesting that acute coronary artery occlusion may significantly increase residual stress and strain in the left ventricle.

Omens et al. [50] showed that physiologic left ventricular remodelling in rats decreases myocardial residual strain in proportion to the relative reduction in wall thickness-radius ratio.

6. Cartilaginous Tissue

Curling of cartilaginous tissue was reported already in 1958 by Gibson and Davis, cf. [58]. Curling behavior was also shown in [57]. The studies on residual stress (sometimes called “interlocked stress” or self-locked stress) in cartilaginous tissues, prove that our knowledge of residual stresses in biological tissues is longer then commonly believed. For review of the experimental results and modelling of cartilage behaviour the reader is referred to [34] and [74].

Part III. Mathematical approach to modelling residual stress

For the introduction and description of the basic mechanical concepts, relevant to the discussion presented in the following sections, the reader is referred to the Appendices A–D.

7. Residually Stressed Elastic Materials

Until now, in our considerations of constitutive modeling, existence of stress-free state (sometimes called natural state) has always been assumed.

Residual stress is the internal stress present in a body, not necessarily elastic, in an unloaded equilibrium configuration. That stress is often the result of the manufacturing process used to form or construct the structure, or may be due to the deformation history of the structure. The presence of a residual stress field can have a profound influence on effective mechanical properties of the structure. Residual stress is commonly studied in the context of metals, where it is usually a product of plastic deformation and where the material is elastic only in small strain range. However, residual stress is present in a wide variety of materials, some of which respond elastically to large deformations, at least in a first approximation. For instance, human and animal bone, heart, arteries and cartilage are biological tissues which are known to support significant residual stress fields, cf. Holzapfel and Ogden [31], Jemioło and Telega [36], Ogden [46], and the relevant references cited therein. Bone tissue is not of interest for us here since it behaves in a geometrically linear way. Residual stress in biological tissue develops through growth and remodeling, and are important to the mechanical function of the tissues, cf. Rachev [54], Skalak et al. [59].

Prediction of the mechanical behavior of a residually stressed body will typically require a constitutive model that explicitly includes the influence of residual stress on deformation. In a series of papers, Hoger and her coworkers proposed general forms of constitutive relationships for residually stressed hyperelastic bodies that are composed of material with identified symmetry, cf. Dyke and Hoger [16], Hoger [28, 29], Johnson and Hoger [37, 38]. The aim of the present section is to familiarise the reader with the main ideas introduced by Hoger and her coworkers.

7.1. Some General Relations

Let us write the constitutive equation for the first (unsymmetric) Piola-Kirchhoff stress tensor as follows

$$\mathbf{P}(\mathbf{x}) = \mathbf{g}(\mathbf{x}, \mathbf{F}(\mathbf{x})). \quad (7.1)$$

The residual stress $\overset{r}{\mathbf{P}}$ is defined as the stress in the *reference configuration*, i.e.,

$$\overset{r}{\mathbf{P}}(\mathbf{x}) = \mathbf{g}(\mathbf{x}, \mathbf{I}). \quad (7.2)$$

In the sequel of the present section, the explicit dependence of the constitutive functions on \mathbf{x} will be suppressed except where its appearance is needed for clarity. We observe that \mathbf{x} refers here to the residually stressed configuration.

For the elastic response to be independent of the observer, the response function \mathbf{g} must satisfy

$$\mathbf{g}(\mathbf{Q}\mathbf{F}) = \mathbf{Q}\mathbf{g}(\mathbf{F})$$

for every $\mathbf{F} \in \mathbb{M}_+^3$ and every proper orthogonal \mathbf{Q} .

The symmetry group of an elastic material at \mathbf{x} is now denoted by \mathcal{G}_x , and is such that

$$\mathbf{g}(\mathbf{x}, \mathbf{F}\mathbf{Q}) = \mathbf{g}(\mathbf{x}, \mathbf{F})\mathbf{Q}$$

for all $\mathbf{F} \in \mathbb{M}_+^3$. Independence of the observer requires that

$$\mathbf{g}(\mathbf{x}, \mathbf{Q}\mathbf{F}\mathbf{Q}^T) = \mathbf{Q}\mathbf{g}(\mathbf{x}, \mathbf{F})\mathbf{Q}^T \tag{7.3}$$

for all $\mathbf{Q} \in \mathcal{G}_x$. By evaluating (7.3) at $\mathbf{F} = \mathbf{I}$, we find that the residual stress $\overset{r}{\mathbf{P}}$ must satisfy

$$\overset{r}{\mathbf{P}}(\mathbf{x})\mathbf{Q} = \mathbf{Q}\overset{r}{\mathbf{P}}(\mathbf{x}) \tag{7.4}$$

for all $\mathbf{Q} \in \mathcal{G}_x$. Hence we conclude that a material with a particular symmetry can support only those residual stress fields that commute with all elements of its symmetry group. From this condition the restrictions on the form of the residual stress appropriate to a specific material symmetry can be obtained.

The relation between the first Piola-Kirchhoff stress and the Cauchy stress $\boldsymbol{\sigma}$ is given by

$$\mathbf{P} = J\boldsymbol{\sigma}\mathbf{F}^{-T}.$$

In the reference configuration $\mathbf{F} = \mathbf{I}$; thus $\overset{r}{\mathbf{P}} = \overset{r}{\boldsymbol{\sigma}}$ or $\overset{r}{\mathbf{P}} = \overset{r}{\mathbf{P}}^T$. Consequently the residual stress $\overset{r}{\mathbf{P}}$ is symmetric.

We will always take the reference configuration to be an unloaded equilibrium state. The residual stress must then satisfy the equilibrium equation

$$\operatorname{div}_x \overset{r}{\mathbf{P}} = \mathbf{0} \quad \text{in } \Omega, \tag{7.5}$$

and the zero traction condition

$$\overset{r}{\mathbf{P}}\mathbf{m} = \mathbf{0} \quad \text{on } \partial\Omega \tag{7.6}$$

where \mathbf{m} is a unit vector normal to $\partial\Omega$. We assume that $\overset{r}{\mathbf{P}}(\mathbf{x})$ is sufficiently regular. To admit a broader class of solutions, Eq. (7.5) may be understood in the weak (variational) sense. Then $\overset{r}{\mathbf{P}}\mathbf{m}$ is the trace of $\overset{r}{\mathbf{P}}$ on $\partial\Omega$; i.e. the trace in the sense of “value” of function from a Sobolev space on $\partial\Omega$. The boundary $\partial\Omega$ may contain edges and corners.

7.1.1. Isotropy. For an isotropic material, according to (7.4), the residual stress must commute with all proper orthogonal tensors. Therefore it is a hydrostatic pressure and because $\mathbf{F} = \mathbf{I}$, we have

$$\overset{r}{\mathbf{P}}(\mathbf{x}) = p(\mathbf{x})\mathbf{I}, \quad \mathbf{x} \in \Omega. \quad (7.7)$$

Equilibrium equation becomes

$$\operatorname{div}_{\mathbf{x}} \overset{r}{\mathbf{P}}(\mathbf{x}) = \nabla_{\mathbf{x}} p(\mathbf{x}) = \mathbf{0},$$

so p is a constant. On account of (7.6) p is identically zero in Ω . The following result has been established: an isotropic body can support no residual stress.

7.1.2. Transverse isotropy The symmetry group of transversely isotropic material is the set of all rotations about the axis of symmetry of the material, so the residual stress must be of the form

$$\overset{r}{\mathbf{P}}(\mathbf{x}) = p(\mathbf{x})\mathbf{I} + q(\mathbf{x})\mathbf{M}(\mathbf{x}) \quad (7.8)$$

where $\mathbf{M}(\mathbf{x}) = \mathbf{v}(\mathbf{x}) \otimes \mathbf{v}(\mathbf{x})$, and $\mathbf{v}(\mathbf{x})$ is a unit vector along the axis of symmetry at \mathbf{x} . The possibility that q is identically zero is excluded; otherwise the material would be isotropic.

The equilibrium equation (7.5) takes the form

$$\nabla_{\mathbf{x}} p(\mathbf{x}) + \mathbf{M}(\mathbf{x})\nabla_{\mathbf{x}} q(\mathbf{x}) + q(\mathbf{x})[(\nabla_{\mathbf{x}} \mathbf{v}(\mathbf{x}))\mathbf{v}(\mathbf{x}) + (\operatorname{div}_{\mathbf{x}} \mathbf{v}(\mathbf{x}))\mathbf{v}(\mathbf{x})] = \mathbf{0}, \quad \text{in } \Omega, \quad (7.9)$$

whilst the boundary condition (7.6) becomes

$$p\mathbf{m} + q(\mathbf{v} \cdot \mathbf{m})\mathbf{m} = \mathbf{0} \quad \text{on } \partial\Omega. \quad (7.10)$$

The last equation is satisfied if and only if at least one of the following holds on $\partial\Omega$:

$$\begin{aligned} p = q = 0, \\ p = 0 \quad \text{and} \quad \mathbf{v} \cdot \mathbf{m} = 0, \\ p + q = 0 \quad \text{and} \quad (\mathbf{v} \cdot \mathbf{m})^2 = 1. \end{aligned}$$

Hoger [28] examined two specific cases: where the axis of symmetry is uniform, and where the parameters p and q are uniform. Moreover, she also investigated full equations (7.9) and (7.10) for the specific body geometry of a right circular cylinder, cf. also Ogden [46]. It is not difficult to show that in these two specific cases we arrive at the following results:

- (i) a transversely isotropic body with uniform axis of symmetry can support no residual stress,
- (ii) a transversely isotropic body can support a nonzero residual stress field with uniform parameters p and q if and only if the axis of symmetry \mathbf{v} satisfies

$$\operatorname{div}_{\mathbf{x}} \mathbf{v}(\mathbf{x}) = 0 \quad \text{and} \quad (\nabla_{\mathbf{x}} \mathbf{v}(\mathbf{x})) \mathbf{v}(\mathbf{x}) = \mathbf{0}$$

throughout the body, and either

$$\mathbf{v}(\mathbf{x}) \cdot \mathbf{m}(\mathbf{x}) = 0$$

at all points $\mathbf{x} \in \partial\Omega$, or

$$[\mathbf{v}(\mathbf{x}) \cdot \mathbf{m}(\mathbf{x})]^2 = 1$$

at all points $\mathbf{x} \in \partial\Omega$. The residual stress possible in each of these two cases is given by equations (7.11) and (7.12):

$$\overset{r}{\mathbf{P}}(\mathbf{x}) = q\mathbf{M}(\mathbf{x}) \tag{7.11}$$

with $\mathbf{m}(\mathbf{x}) \cdot \mathbf{v}(\mathbf{x}) = 0$, $\mathbf{x} \in \partial\Omega$;

$$\overset{r}{\mathbf{P}}(\mathbf{x}) = p[\mathbf{I} - \mathbf{M}(\mathbf{x})] \tag{7.12}$$

with $[m(\mathbf{x}) \cdot \mathbf{v}(\mathbf{x})]^2 = 1$, $\mathbf{x} \in \partial\Omega$.

Hoger [28] considered also bodies with crystal symmetries, like cubic, tetragonal, hexagonal, and rhombic.

7.1.3. The virtual configuration. Prior to passing to constitutive modeling of residually stressed elastic materials we will discuss the concept of virtual configuration introduced and developed by Johnson and Hoger [38]. According to the last paper, the derivation of the constitutive equation in the considered case is based on the idea that for each infinitesimal neighborhood in the residually stressed body there exists a corresponding stress free configuration. In the general case the stress free configuration is attained in the limit as the volume of the neighborhood tends to zero, so this stress free configuration can be thought of as a point. This stress free configuration can be used to derive the constitutive equation for the corresponding point in the residually stressed body. The stress free configuration of a part of a body

is referred to as the “virtual configuration” of that part. We note that the virtual configuration provides only a physical interpretation of the mathematics employed in the derivation. Thus the adjective “virtual” emphasizes that this configuration is a conceptualization. The geometry of the virtual configuration need not be determined explicitly, and the virtual configuration need not be attainable experimentally. To be consistent with standard terminology, we will refer to material that supports no stress as natural material; thus, a virtual configuration is composed of natural material.

The use of a virtual configuration for the derivation of the constitutive equation *does not imply* that the residual stress is actually a result of a prior elastic deformation. Consequently, this method *cannot* be thought of as a superposition of two (possibly finite) deformations, where the residually stressed body is just an intermediate configuration in the deformation. This is made especially clear by the fact that the (mathematically) constructed virtual configuration does not physically exist for most residually stressed elastic bodies, cf. Hoger [29].

Let part $\overset{r}{R}_\varepsilon$ of the residually stressed body, in the configuration $\overset{r}{\Omega}$, be a spherical neighborhood which is centered at $\bar{\mathbf{x}}$ and has radius ε . The boundary of the part, $\partial\overset{r}{R}_\varepsilon$, has outward unit normal $\overset{r}{\mathbf{n}}$ for every value of ε . The tractions $\overset{r}{\boldsymbol{\sigma}}\overset{r}{\mathbf{n}}$ is imposed on the boundary $\partial\overset{r}{R}_\varepsilon$ by the rest of the body. If these tractions could be removed, the part $\overset{r}{R}_\varepsilon$ would deform into the configuration R_ε . This deformation is denoted by $\overset{r}{\mathbf{y}}_\varepsilon^{-1}$, and, for each ε , $\overset{r}{\mathbf{y}}_\varepsilon^{-1}$ is defined so that the image of the point \mathbf{x} is always the point $\overset{v}{\mathbf{x}} = \overset{r}{\mathbf{y}}_\varepsilon^{-1}(\bar{\mathbf{x}})$; *v*-means “virtual”. Obviously, in the limit, as ε approaches zero, the region R_ε degenerates to a point at $\overset{v}{\mathbf{x}}$. The configuration R_ε supports the residual stress field $\overset{r'}{\boldsymbol{\sigma}}_\varepsilon$, which in general is not zero. Johnson and Hoger [38] proved that $\lim_{\varepsilon \rightarrow 0} \overset{r'}{\boldsymbol{\sigma}}_\varepsilon = \mathbf{0}$, so the material at the point $\overset{v}{\mathbf{x}}$ is a stress free configuration of $\bar{\mathbf{x}} \in \overset{r}{\Omega}$ in the limit as ε approaches zero. In essence, the proof is based on Signorini’s mean stress theorem, i.e. the volume average $\overset{r'}{\boldsymbol{\sigma}}'_M(R_\varepsilon)$ of $\overset{r'}{\boldsymbol{\sigma}}_\varepsilon$ is calculated first. Exploiting next simple properties of the mean value $\overset{r'}{\boldsymbol{\sigma}}'_M(R_\varepsilon)$ and performing some estimations, under physically plausible regularity assumptions, we arrive at the desired result.

As we already know Johnson and Hoger [38] refer to the stress free configuration of a part of $\overset{r}{\Omega}$ (the residually stressed configuration) as the virtual configuration, R_v say. Let the virtual configuration of $\overset{r}{\Omega}$ be denoted by $\overset{r}{\bar{B}}_v$,

and define it as the closure of the union of the virtual configuration R_{v_i} :

$$\overline{B}_v = \bigcup_{i=1}^K R_{v_i}.$$

Obviously, K is finite for residually stressed bodies in special cases only, and infinite for the typical residually stressed body. When K is infinite the virtual configuration R_v has no volume and therefore cannot exist physically. However, such a virtual configuration can be *approximated experimentally*, cf. Johnson and Hoger [38].

Consider a deformation $\widehat{\mathbf{y}}$ defined on the residually stressed configuration. When $\varepsilon > 0$, the deformation \mathbf{y}_ε^* , which maps R_ε into the deformed configuration is the composition of $\widehat{\mathbf{y}}$ and \mathbf{y}_ε^r for all point in R_ε

$$\mathbf{y}_\varepsilon^* = \widehat{\mathbf{y}} \circ \mathbf{y}_\varepsilon^r,$$

so

$$\nabla \mathbf{y}_\varepsilon^* = \nabla \widehat{\mathbf{y}} \nabla \mathbf{y}_\varepsilon^r \tag{7.13}$$

in R_ε . For the sake of simplicity the arguments of functions appearing in (7.13) have been omitted. The limits of $\nabla \mathbf{y}_\varepsilon^*$ and $\nabla \mathbf{y}_\varepsilon^r$, are well defined as ε approaches zero, cf. Johnson and Hoger [38].

So, with the definitions:

$$\mathbf{F}^r = \lim_{\varepsilon \rightarrow 0} \nabla \mathbf{y}_\varepsilon^r(\mathbf{x}), \tag{7.14}$$

$$\mathbf{F}^* = \lim_{\varepsilon \rightarrow 0} \nabla \mathbf{y}_\varepsilon^*(\mathbf{x}), \tag{7.15}$$

and

$$\mathbf{F}^* = \mathbf{F}^r \mathbf{F}. \tag{7.16}$$

Since the elastic material at \mathbf{x}^v is stress free, the applicable constitutive equation for the deformations \mathbf{y}_ε^r and \mathbf{y}_ε^* , in the limit as ε tends to zero, is the constitutive equation of the natural material: $\boldsymbol{\sigma} = \mathbf{g}(\mathbf{F})$. We observe that the tensors \mathbf{F}^r and \mathbf{F}^* have clear physical meanings as the deformation gradients (relative to the virtual, or natural, configuration) that produce the residual stress $\boldsymbol{\sigma}^r$ at the point $\bar{\mathbf{x}}$ in Ω , and the stress $\boldsymbol{\sigma}$ at the point $\mathbf{y} = \mathbf{y}^*(\bar{\mathbf{x}})$ in Ω_t , respectively. Thus we have

$$\boldsymbol{\sigma}^r = \mathbf{g}(\mathbf{F}^r) \tag{7.17}$$

and

$$\boldsymbol{\sigma} = \mathbf{g}(\mathbf{F}^*) \quad (7.18)$$

More precisely, the function \mathbf{g} depends explicitly on the position in the body.

7.2. Derivation of the Constitutive Relationships

Following Hoger [29] and Johnson and Hoger [38] we shall briefly describe the derivation of constitutive equations for residually stressed material.

7.2.1. General approach. From our previous discussion it follows that the Cauchy stress $\boldsymbol{\sigma}$ in the deformed configuration is given by a response function, $\widehat{\mathbf{g}}$ say, of the deformation gradient $\mathbf{F}(\mathbf{x})$, $\mathbf{x} \in \overset{r}{\Omega}$, and the residual stress $\overset{r}{\boldsymbol{\sigma}}$:

$$\boldsymbol{\sigma} = \widehat{\mathbf{g}}(\mathbf{F}, \overset{r}{\boldsymbol{\sigma}}). \quad (7.19)$$

We observe that it is not assumed that the process that originally produced the residual stress was elastic.

The form (7.19) of the constitutive equation requires the inversion of the constitutive relationship relating $\overset{r}{\boldsymbol{\sigma}}$ with an appropriate strain measure. Two specific cases will now be considered.

7.2.2. Isotropic natural material. Suppose that the residual stress is known, and the underlying *natural material* is isotropic. It does not imply, however, that the residual stresses in the configuration $\overset{r}{\Omega}$ are isotropic.

From Section 10.2 we know that for an isotropic material we have

$$\boldsymbol{\sigma} = \mathbf{g}(\mathbf{F}) = \mathbf{g}(\mathbf{V}). \quad (7.20)$$

In terms of $\mathbf{B} = \mathbf{F}\mathbf{F}^T = \mathbf{V}^2$, we get

$$\boldsymbol{\sigma} = \overline{\mathbf{g}}(\mathbf{B}). \quad (7.21)$$

The polar decomposition of $\overset{r}{\mathbf{F}}$ yields

$$\overset{r}{\mathbf{F}} = \overset{r}{\mathbf{V}}\overset{r}{\mathbf{R}}.$$

Thus (7.20) and (7.21) give

$$\overset{r}{\boldsymbol{\sigma}} = \mathbf{g}(\overset{r}{\mathbf{F}}) = \overline{\mathbf{g}}(\overset{r}{\mathbf{B}}). \quad (7.22)$$

On account of (7.16) the gradient $\overset{*}{\mathbf{F}}$ from the virtual configuration to the deformed configuration of the body may be written as

$$\overset{*}{\mathbf{F}} = \overset{r}{\mathbf{F}}\overset{r}{\mathbf{F}} = \overset{r}{\mathbf{R}}\overset{r}{\mathbf{U}}\overset{r}{\mathbf{V}}\overset{r}{\mathbf{R}}. \tag{7.23}$$

Hence

$$\overset{*}{\mathbf{B}} = \overset{*}{\mathbf{F}}\overset{*}{\mathbf{F}}^T = \overset{r}{\mathbf{F}}\overset{r}{\mathbf{B}}\overset{r}{\mathbf{F}}^T. \tag{7.24}$$

Recall that the principle of material frame indifference requires that the response function satisfies the condition:

$$\mathbf{g}(\mathbf{F}) = \mathbf{R}\mathbf{g}(\mathbf{U})\mathbf{R}^T. \tag{7.25}$$

The response function can equally be written in terms of \mathbf{C} as follows

$$\tilde{\mathbf{g}}(\mathbf{C}) = \mathbf{g}(\sqrt{\mathbf{C}}) = \mathbf{g}(\mathbf{U}). \tag{7.26}$$

From (7.21), (7.24)–(7.26) we get

$$\boldsymbol{\sigma} = \overset{*}{\mathbf{g}}(\overset{*}{\mathbf{B}}) = \overset{r}{\mathbf{g}}(\overset{r}{\mathbf{F}}\overset{r}{\mathbf{B}}\overset{r}{\mathbf{F}}^T) = \mathbf{R}\overset{r}{\mathbf{g}}(\overset{r}{\mathbf{U}}\overset{r}{\mathbf{B}}\overset{r}{\mathbf{U}})\mathbf{R}^T. \tag{7.27}$$

Hoger [29] assumes that $\overset{r}{\mathbf{g}}$ is locally invertible. Then, on a neighborhood of $\overset{r}{\mathbf{B}}$, there is an isotropic function $\mathbf{h} = \overset{r}{\mathbf{g}}^{-1}$ such that at each point of the body (7.22) can be inverted as

$$\overset{r}{\mathbf{B}} = \mathbf{h}(\overset{r}{\boldsymbol{\sigma}}). \tag{7.28}$$

Finally, from the last relation and (7.27), the Cauchy stress at $\mathbf{y} = \hat{\mathbf{y}}(\mathbf{x}, t) \in \Omega_t$ can be written as

$$\boldsymbol{\sigma} = \mathbf{R}\overset{r}{\mathbf{g}}(\mathbf{U}\mathbf{h}(\overset{r}{\boldsymbol{\sigma}})\mathbf{U})\mathbf{R}^T. \tag{7.29}$$

Since $\mathbf{U} = \mathbf{R}^{-1}\mathbf{F}$, the constitutive equation for the residually stressed body, isotropic in the natural (virtual) configuration is thus of the form (7.19).

If $\overset{r}{\mathbf{g}}$ is not locally invertible, then the Cauchy stress $\boldsymbol{\sigma}$ in the deformed configuration Ω_t is a function of \mathbf{U} and $\overset{r}{\mathbf{B}}$, like in (7.27) or a function of other strain measures.

Remark

- (i) The natural Mooney-Rivlin (incompressible) material is described by the following constitutive relationship:

$$\boldsymbol{\sigma} = -p\mathbf{I} + 2c_1\mathbf{B} - 2c_2\mathbf{B}^{-1},$$

where c_1 and c_2 are material coefficients. It is known that the constitutive relationship for a Mooney-Rivlin material is invertible, see Johnson and Hoger [38] for details.

The Cauchy stress tensor $\boldsymbol{\sigma}$ in the deformed configuration Ω_t is now given by

$$\boldsymbol{\sigma} = -p\mathbf{I} + 2c_1\mathbf{F}\mathbf{B}\mathbf{F}^T - 2c_2\mathbf{F}^{-T}\mathbf{B}^{r-1}\mathbf{F}^{-T}. \quad (7.30)$$

To obtain the constitutive equation (7.30) in the form (7.19) one has to perform the inversion of:

$$\overset{r}{\boldsymbol{\sigma}} = -\overset{r}{p}\mathbf{I} + 2c_1\overset{r}{\mathbf{B}} - 2c_2\overset{r}{\mathbf{B}}^{-1}. \quad (7.31)$$

This was done by Johnson and Hoger [38].

- (ii) Hoger [29] considered also the case where the underlying natural material is transversely isotropic. The calculation is still algebraic, though lengthy.
- (iii) The method presented by Hoger [29] for transverse isotropy can be generalized for any material symmetry with known basic invariants. For more details the reader is referred to the paper by Hoger [29].

8. Conclusion

The residual stress is present in a large range of biological tissues in physiological conditions. It usually builds up during the process of growth of tissue or its adaptation to changing environment. Although researchers were aware of these processes for a long time, the experimental evidence of the existence of the residual stress has been brought to light relatively recently. These findings led to a number of mathematical models aiming at calculation of the residual stress in a given (physiological or pathological) conditions, which are described in the present paper.

The knowledge of the residual stress in the living tissue is no less important than in case of engineering materials because the state of this residual stress influences the biological mechanisms of remodelling and adaptation of the tissue. In that respect, the mechanical problem of finding the residual stress field and the biological problem of tissue remodelling are inseparable.

References

1. T. ADACHI, M. TANAKA, and Y. TOMITA, *Uniform stress in bone structure with residual stress*, J. Biomech. Eng. **120**:342–347, 1998
2. A. ASCENZI and A. BENVENUTI, *Evidence of a state of initial stress in osteonic lamellae*, J. Biomech. **19**:447–453, 1977
3. A. ASCENZI, A. BENVENUTI, A. BIGI, E. FORESTI, M.H.J. KOCH, F. MANGO, A. RIPAMONTI, and N. ROVERI, *X-ray diffraction on cyclically loaded osteons*, Calcif. Tissue Int. **62**:266–273, 1998
4. M.-G. ASCENZI, *A first estimation of prestress in so-called circulatory fibered osteonic lamellae*, J. Biomech. **32**:935–942, 1999
5. D.H. BERGEL, *The residual properties of the arterial wall*, London 1960
6. A. BOCHENEK and M. REICHER, *Human anatomy, Vol. 3: Vascular system* (in Polish), Państwowy Zakład Wydawnictw Lekarskich Warszawa 1978
7. V. CAGLIOTI, *Sulla struttura delle ossa*, Atti. Congr. naz. Clin. pura ed appl., pp.320–331, 1935
8. C.J. CHUONG and Y.C. FUNG, *Three-dimensional stress distribution in arteries*, J. Biomech. Eng. **105**:268–274, 1983
9. C.J. CHUONG and Y.C. FUNG, *On residual stress in arteries*, J. Biomech. Eng. **108**:189–192, 1986
10. C.J. CHUONG and Y.C. FUNG, *Residual stress in arteries*, In G.W. Schmid-Schönbein, S.L.-Y. Woo, and B.W. Zweifach [eds.], *Frontiers in Biomechanics*, pp.117–129, Springer-Verlag, Berlin 1986
11. P.G. CIARLET, *Mathematical elasticity*, North Holland, Amsterdam 1988
12. S.C. Cowin [ed.] *Bone Mechanics Handbook*, CRC Press, Boca Raton 2001
13. J.D. CURREY, *Bones: Structure and Mechanics*, Princeton University Press, Princeton 2002

14. A. DELFINO, N. STERGIOPULOS, J.E. MOORE, and J.-J. MEISTER, *Residual strain effects on the stress field in a thick wall finite element model of the human carotid bifurcation*, J. Biomech., **30**:777–786, 1997
15. A. DORFMAN and A. MUHR [eds.], *Constitutive models for rubber, Proc. The First European Conference on Constitutive Models for Rubber, held in Vienna 9-10 September 1999*, pages 23–28, Rotterdam-Brookfield, Balkema 1999
16. T.J. VAN DYKE, *A new method for predicting the opening angle for soft tissue*, J. Biomech. Eng. **124**:347–354, 2002
17. P. FRIDEZ, M. ZULLIGER, F. BOBARD, G. MONTORZI, H. MIYAZAKI, K. HAYASHI, and N. STERGIOPULOS, *Geometrical, functional, and histomorphometric adaptation of rat carotid artery in induced hypertension*, J. Biomech. **36**:671–680, 2003
18. Y. C. FUNG, *Biomechanics: Circulation*, Springer-Verlag, New York 1997
19. Y.C. FUNG and S.Q. LIU, *Change of residual strains in arteries due to hypertrophy caused by aortic constriction*, Circulation Res. **65**:1340–1349, 1989
20. Y.C. FUNG and S.Q. LIU, *Changes of zero-stress state of rat pulmonary arteries in hypotoxic hypertension*, J. Appl. Physiol. **70**:2455–2470, 1991
21. Y.C. FUNG, *Biomechanics, mechanical properties of living tissues*, second, enlarged and revised edition, Springer-Verlag, Berlin–New York 1993
22. F.A.M.W. GEBHARDT, *Über funktionell wichtige Anordnungsweisen der größeren und feineren Bauelemente des Wirbeltierknochen. I. Allgemeiner Teil*, Arch. Entw. Mech. **12**:1–52, 1901
23. S.E. GREENWALD, J.E. MOORE, A. RACHEV, T.P.C. KANE, and J.-J. MEISTER, *Experimental investigation of the distribution of residual strains in the artery wall*, J. Biomech. Eng. **119**:439–444, 1997
24. H. GREGERSEN, T.C. LEE, S. CHIEN, R. SKALAK, and Y.C. FUNG, *Strain distributin in the layered wall of the esophagus*, J. Biomech. Eng. **121**:442–448, 1999

25. H.-C. HAN, L. ZHAO., M. HUANG, L.-S. HOU, Y.-T. HUANG, and Z.-B. KUANG, *Postsurgical changes of the opening angle of canine autogenous vein graft*, *J. Biomech. Eng.* **120**: 211–216, 1998
26. H.C. HAN and Y.C. FUNG, *Direct measurement of transverse residual strains in aorta*, *Am. J. Physiol.* **270**: H750–H759, 1996
27. K. HAYASHI, *Residual stress in living materials*, In H. Fujiwara, T. Abe, and K. Tanaka [eds.], *Residual stress III: Science and Technology* volume 1, pp.121–127, Elsevier Applied Science, New York 1992
28. A. HOGER, *On the residual stress possible in an elastic body with material symmetry*, *Arch. Rat. Mech. Anal.* **88**: 271–289, 1985
29. A. HOGER, *Virtual configurations and constitutive equations for residually stressed bodies with material symmetry*, *J. Elasticity* **48**: 125–144, 1997
30. G.A. HOLZAPFEL, *Structural and numerical models for the (visco)elastic response of arterial walls with residual stresses*, In G.A. Holzapfel and R.W. Ogden [eds.], *Biomechanics of Soft Tissue, CISM Courses and Lectures*, Springer-Verlag, Wien–New York 2002
31. G.A. HOLZAPFEL and R.W. OGDEN [eds.], *Biomechanics of Soft Tissue, CISM Courses and Lectures*, Springer-Verlag, Wien–New York 2003
32. J.D. HUMPHREY, *Remodeling of collagenous tissue at fixed lengths*, *J. Biomech. Eng.* **121**: 591–597, 1999
33. J.D. HUMPHREY, *Cardiovascular Solid Mechanics: Cells, Tissues and Organs*, Springer Verlag, New York 2002
34. J.M. HUYGHE and P.H.M. BOVENDEERD, *Biological Mixtures*, in: AMAS Lecture Notes **20**, *Modelling Coupled Phenomena in Saturated Porous Materials*, pp.227–276, Warszawa-Bydgoszcz 2004.
35. S. JEMIOŁO and J.J. TELEGA, *Representations of tensor functions and applications in continuum mechanics*, *IFTR Reports*, **3**, 1997
36. S. JEMIOŁO and J.J. TELEGA, *A pseudo-hyperelastic model of soft tissues*, *Acta Bioeng. Biomech.*, Vol. 3(Supp. 1), pp.208–216, 2001.

37. B.E. JOHNSON and A. HOGER, *The dependence of the elasticity tensor on residual stress*, J. Elasticity **33**: 145–165, 1993
38. B.E. JOHNSON and A. HOGER, *The use of virtual configuration in formulating constitutive equations for residually stressed elastic materials*, J. Elasticity **41**: 177–215, 1995
39. S.Q. LIU and Y.C. FUNG, *Zero-stress state of arteries*, J. Biomech. Eng. **110**: 82–84, 1988
40. S.Q. LIU and Y.C. FUNG, *Relationship between hypertension, hypertrophy, and opening angle of zero-stress state of arteries following aortic constriction*, J. Biomech. Eng. **111**: 325–335, 1989
41. T. MATSUMOTO, T. GOTO, T. FURUKAWA, and M. SATO, *Residual stress and strain in the lamellar unit of the porcine aorta: experiment and analysis*, J. Biomech. **37**: 807–815, 2004
42. T. MATSUMOTO and K. HAYASHI, *Response of arterial wall to hypertension and residual stress*, In K. Hayashi, A. Kamiya, and K. Ono [eds.], *Biomechanics—Functional Adaptation and Remodelling*, Springer-Verlag, Tokyo 1996
43. J.-J. MEISTER, *Residual strains effects on the stress field in a thick wall finite element model of the human carotid bifurcation*, J. Biomech. **30**: 777–786, 1997
44. N. NUÑO and G. AVANZOLINI, *Residual stresses at the stem-cement interface of an idealized cemented hip cement*, J. Biomech. **35**: 849–852, 2002
45. R.W. OGDEN, *Non-linear Elastic Deformations*, Dover Publications, New York 1997
46. R.W. OGDEN, *Nonlinear Elasticity with Application to Material Modelling, Lecture Notes*, **6**, Centre of Excellence for Advanced Materials and Structures, AMAS, IFTR PAS Warsaw, Poland 2003
47. R.W. OGDEN and C.A.J. SCHULZE-BAUER, *Phenomenological and structural aspects of the mechanical response of arteries*, In J. Casey and G. Bao [eds.], *Mechanics in Biology*, vol. AMD-242, BED-46, pp.125–140, The American Society of Mechanical Engineers, New York 2000

48. T. OKUYAMA and H. YAMAMOTO, *Residual stress in living tree*, In H. Fujiwara, T. Abe, and K. Tanaka [eds.], *Residual stress III: Science and Technology*, pp.128–133, Elsevier Applied Science, New York 1992
49. J.H. OMENS and Y.-C. FUNG, *Residual strain in rat left ventricle*, *Circulation Res.* **66**:37–45, 1990
50. J.H. OMENS, S.M. VAPLON, B. FAZELI, and A.D. MCCULLOCH, *Left ventricular geometric remodeling and residual stress in the rat heart*, *J. Biomech. Eng.*, **120**:715–719, 1998
51. J.H. OMENS, A.D. MCCULLOCH, and J.C. CRISCIONE, *Complex distribution of residual stress and strains in the mouse left ventricle: experimental and theoretical models*, *Biomechan. Model. Mechanobiol.* **1**:267–277, 2003
52. P. PATITUCCI, *Computer program for fitting pseudo-strain energy functions to soft tissue experimental stress and strain data*, Digital Equipment Users Society, DECUS, One Iron Way Marlboro, Massachusetts 1982 pp.11–548
53. A. RACHEV, N. STERGIOPULOS, and J.-J. MEISTER, *A model for geometric and mechanical adaptation of arteries to sustained hypertension*, *J. Biomech. Eng.*, **120**:9–17, 1998
54. A. RACHEV, *A model of arterial adaption to alterations in blood flow*, *J. Elasticity* **61**:83–111, 2000
55. A. RACHEV and S.E. GREENWALD, *Residual strains in conduit arteries*, *J. Biomech.* **36**:661–670, 2003
56. Y. SEGUCHI, *Preliminary study on adaptation by remodeling*, *Tissue Engineering*, page 75, 1989
57. L.A. SETTON, H. TOHYAMA, and V.C. MOW, *Swelling and curling behaviors of articular cartilage*, *J. Biomech. Eng.* **120**:355–361, 1998
58. F.H. SILVER and G. BRADICA, *Mechanobiology of cartilage: how do internal and external stress affect mechanochemical transduction and elastic energy storage?*, *Biomechan. Model. Mechanobiol.* **1**:219–238, 2002

59. R. SKALAK, S. ZARGARYAN, R.K. JAIN, P.A. NETTI, and A. HOGER, *Compatibility and the genesis of residual stress by volumetric growth*, *J. Math. Biol.* **34**: 889–914, 1996
60. M. STAŃCZYK, *Thermal problems in orthopaedic biomechanics* [in Polish], PhD thesis Institute of Fundamental Technological Research, Polish Academy of Sciences Warsaw, Poland 2004
61. S.R. SUMMEROUR, J.L. EMERY, B. FAZELI, J.H. OMENS, and A.D. MCCULLOCH, *Residual strain in ischemic ventricular myocardium*, *J. Biomech. Eng.*, **120**: 710–714, 1998
62. L.A. TABER, *A model of aortic growth based on fluid shear and fiber stresses*, *J. Biomech. Eng.* **120**: 348–354, 1998
63. L.A. TABER and S. CHABERT, *Theoretical and experimental study of growth and remodeling in the developing heart*, *Biomech. Modeling Mechanobiol.* **1**: 29–43, 2002
64. L.A. TABER and J.D. HUMPHREY, *Stress-modulated growth, residual stress, and vascular heterogeneity*, *J. Biomech. Eng.* **123**: 528–535, 2001
65. K. TAKAMIZAWA and K. HAYASHI, *Constitutive law of the arterial wall and stress distribution*, In G. Yagawa and S.N. Atluri [eds.], *Computational Mechanics'86: Theory and Applications*, Proc. Int. Conf. Computational Mechanics, May 25-29, pp. IV-149–IV-154, Springer-Verlag, Tokyo 1986
66. K. TAKAMIZAWA and K. HAYASHI, *Strain energy density function and uniform strain hypothesis for arterial mechanics*, *J. Biomech.* **20**: 7–17, 1987
67. K. TAKAMIZAWA and K. HAYASHI, *Uniform strains hypothesis and thin-walled theory in arterial mechanics*, *Biorheology* **25**: 555–565, 1988
68. K. TAKAMIZAWA and T. MATSUDA, *Kinematics for bodies undergoing residual stress and its applications to the left ventricle*, *J. Appl. Mech.* **57**: 321–329, 1990
69. M. TANAKA and T. ADACHI, *Preliminary study on mechanical remodeling permitting residual stress*, *JSME Int. J.* **37**: 87–95, 1994

70. M. TANAKA and T. ADACHI, *Model and simulation of bone remodeling considering residual stress*, In K. Hayashi and H. Ishikawa [eds.], *Computational Biomechanics*, pp.3–21, Springer, Tokyo 1996
71. M. TANAKA and T. ADACHI, *Residual stress in bone structure: experimental observation on model study with uniform stress hypothesis*, In K. Hayashi and K. Ono [eds.], *Biomechanics—Functional Adaptation and Remodeling*, pp.169–184, Springer-Verlag, Tokyo 1996
72. M. TANAKA, T. ADACHI, Y. SEGUCHI, and Y. MORIMOTO, *Residual stress of biological tissues and model of adaptation by remodeling*, In H. Fujiwara, T. Abe, and K. Tanaka [eds.], *Residual stress III: Science and Technology*, volume 1, pp.134–139, Elsevier Applied Science, New York 1992
73. M. TANAKA, T. ADACHI, and Y. TOMITA, *Mechanical remodeling of bone structure considering residual stress*, *JSME Int. J.* **39** : 297–305, 1996
74. J.J. TELEGA and R. WOJNAR, *Streaming potentials in biological tissues*, in: *AMAS Conference Proceedings 5*, Orthopaedic Biomechanics, pp.383–453, Warszawa 2003.
75. R.N. VAISHNAV and J. VOSSOUGH, *Residual stress and strain in aortic segments*, *J. Biomech.* **20** : 235–239, 1987
76. R.S. VAISHNAV and J. VOSSOUGH, *Estimation of residual strains in aortic segments*, In C.W. Hall [ed.], *Biomedical Engineering II, Recent Developments*, pp.330–333, Pergamon Press, New York 1983
77. J. VALENTA, T. HURUŠ, M. SOCHOR, R. ČIHÁK, C. POVÝŠIL, and J. STEIDL, *Residual stresses in the human aorta and their influences by growth and remodelling*, *Bio-Medical Mater. Eng.* **7** : 159–169, 1997
78. J. VOSSOUGH, Z. HEDJAZI, and F.S. BORRIS, *Intimal residual stress and strain in large arteries*, In *BED, 1993 Bioengineering Conference*, ASME, Vol. 34, pp.434–437, 1993
79. H. WEINANS, R. HUISKES, and H.J. GROOTENBOER, *Effect of material properties of femoral hip components on bone remodelling*, *J. Orthop. Res.* **10** : 845–853, 1992

80. J.J. WENTZEL, F.J.H. GIJSEN, N. STERGIOPULOS, P.W. SERRUYS, C.J. SLAGE, and R. KRAMS, *Shear stress, vascular remodeling and neointimal formation*, J. Biomech. **36**:681–688, 2003
81. Q.-S. ZHENG, *Theory of representations for tensor functions—a unified invariant approach to constitutive equations*, Appl. Mech. Rev., **47**:545–587, 1994

A. Kinematics

Let \mathbf{x} and \mathbf{y} , respectively, denote the position vector of a material point in some reference configuration, denoted Ω , and the (deformed) current configuration denoted by Ω_t , which may vary with time t . The motion (or time-dependent deformation) from Ω to Ω_t is known when \mathbf{y} is specified as a function of \mathbf{x} and t . Then we write

$$\mathbf{y} = \widehat{\mathbf{y}}(\mathbf{x}, t) \quad (\text{A.1})$$

where $\widehat{\mathbf{y}}$ is the function describing the motion. For each t , $\widehat{\mathbf{y}}$ is invertible and satisfies appropriate regularity conditions.

The deformation gradient tensor, denoted $\mathbf{F}(\mathbf{x}, t)$, is given by

$$\mathbf{F} = \nabla_{\mathbf{x}} \widehat{\mathbf{y}}(\mathbf{x}, t) \quad (\text{A.2})$$

and has Cartesian coordinates $F_{ij} = \partial y_i / \partial x_j$, where y_i and x_j are the components of \mathbf{y} and \mathbf{x} , respectively, $i, j = 1, 2, 3$. Local invertibility of deformation requires that \mathbf{F} be non-singular and the usual convention that

$$J \equiv \det \mathbf{F} > 0 \quad (\text{A.3})$$

is adopted, wherein J is defined.

The inverse of $\widehat{\mathbf{y}}(\mathbf{x}, t)$, t -fixed, is

$$\mathbf{x} = \widehat{\mathbf{y}}^{-1}(\mathbf{y}, t) \quad \forall \mathbf{y} \in \Omega_t \quad (\text{A.4})$$

where $\mathbf{x} \in \Omega$.

A motion is said to be *rigid* if the distance between any two particles of Ω does not change during the motion. The rigid motion is defined by

$$\mathbf{y} := \widehat{\mathbf{y}}(\mathbf{x}, t) = \mathbf{Q}(t)\mathbf{x} + \mathbf{c}(t) \quad (\text{A.5})$$

where $\mathbf{Q}(t)$ is a proper orthogonal second-order tensor and $\mathbf{c}(t)$ is a translation vector.

In the case of Ω the position vector \mathbf{x} and time t serve as independent variables, and the fields are then said to be defined in terms of the referential, material or Lagrangian description. Similarly, in the case of Ω_t , \mathbf{y} and t are used and the description is said to be spatial or Eulerian.

The velocity \mathbf{v} and acceleration \mathbf{a} of a material particle are given, respectively, by

$$\mathbf{v} = \frac{\partial \hat{\mathbf{y}}}{\partial t}(\mathbf{x}, t), \quad \mathbf{a} = \frac{\partial^2 \hat{\mathbf{y}}}{\partial t^2}(\mathbf{x}, t) \tag{A.6}$$

these being the first and second *material time derivatives* of $\hat{\mathbf{y}}$.

We already know that $\det \mathbf{F} \neq 0$, cf. (A.3). Hence \mathbf{F} has an inverse \mathbf{F}^{-1} , given by

$$\mathbf{F}^{-1} = \nabla_{\mathbf{y}} \mathbf{x} \tag{A.7}$$

with components

$$(\mathbf{F}^{-1})_{ij} = \frac{\partial x_i}{\partial y_j}. \tag{A.8}$$

Indeed, a straightforward calculation yields

$$(\mathbf{F}\mathbf{F}^{-1})_{ij} = F_{ik}(\mathbf{F}^{-1})_{kj} = \frac{\partial y_i}{\partial x_k} \frac{\partial x_k}{\partial y_j} = \frac{\partial y_i}{\partial y_j} = \delta_{ij}.$$

We have

$$F_{ij} dx_j = \frac{\partial y_i}{\partial x_j} dx_j = dy_i,$$

i.e.,

$$d\mathbf{y} = \mathbf{F} d\mathbf{x}, \tag{A.9}$$

which has inverse

$$d\mathbf{x} = \mathbf{F}^{-1} d\mathbf{y}. \tag{A.10}$$

Equation (A.9) describes how small *line elements* $d\mathbf{x}$ of material at \mathbf{x} transform under the deformation into $d\mathbf{y}$ (which consists of the same material as $d\mathbf{x}$) at \mathbf{x} . It shows that line elements transform linearly since \mathbf{F} depends on \mathbf{x} , and not on $d\mathbf{x}$. Thus, at each \mathbf{x} , \mathbf{F} is a *linear mapping* (i.e. a second-order tensor).

We justify taking \mathbf{F} to be *non-singular* ($\det \mathbf{F} \neq 0$) by noting that $\mathbf{F} d\mathbf{x} \neq \mathbf{0}$, i.e. a line element cannot be annihilated by the deformation process.

Let ϕ be a scalar field defined on Ω_t , i.e. $\phi(\mathbf{y}, t)$. Since $\mathbf{y} = \hat{\mathbf{y}}(\mathbf{x}, t)$ we may write

$$\phi(\mathbf{y}, t) = \phi[\hat{\mathbf{y}}(\mathbf{x}, t), t] \equiv \Phi(\mathbf{x}, t) \quad (\text{A.11})$$

which defines the notation Φ .

The *material derivative* of ϕ is the rate of change of ϕ at fixed material point P , i.e. at fixed \mathbf{x} . Usually, the material derivative is written $D\phi/Dt$. Performing simple calculation and using (A.6)₁, (A.11) we get

$$\frac{D\phi}{Dt} = \frac{\partial\phi}{\partial t} + \mathbf{v} \cdot \nabla_{\mathbf{y}}\phi. \quad (\text{A.12})$$

Sometimes the notation $\dot{\phi}$ is used instead of $D\phi/Dt$.

Similarly, in the spatial description the acceleration \mathbf{a} is given by

$$\mathbf{a} = \frac{D\mathbf{v}}{Dt} = \frac{\partial\mathbf{v}}{\partial t} + (\mathbf{v} \cdot \nabla_{\mathbf{y}})\mathbf{v}. \quad (\text{A.13})$$

Let ϕ , \mathbf{u} , \mathbf{T} respectively be scalar, vector, and second-order tensor fields associated with a moving body. The following useful formula hold:

$$\begin{aligned} \nabla_{\mathbf{x}}\phi &= \mathbf{F}^T \nabla_{\mathbf{y}}\phi, & \nabla_{\mathbf{x}}\mathbf{u} &= (\nabla_{\mathbf{y}}\mathbf{u})\mathbf{F}, \\ \operatorname{div}_{\mathbf{x}}\mathbf{u} &= J \operatorname{div}_{\mathbf{y}}(J^{-1}\mathbf{F}\mathbf{u}), & \operatorname{div}_{\mathbf{x}}\mathbf{T} &= J \operatorname{div}_{\mathbf{y}}(J^{-1}\mathbf{F}\mathbf{T}). \end{aligned} \quad (\text{A.14})$$

We recall that $J = \det \mathbf{F}$.

Let us pass now to the deformation of area and volume elements. First, consider a surface S in Ω which deforms into the surface S_t in Ω_t . Let $\mathbf{x} \in S$ and let \mathbf{y} be the corresponding point on S_t . By $d\mathbf{x}_1$ and $d\mathbf{x}_2$ we denote line elements of material on S based at \mathbf{x} with images $d\mathbf{y}_1$ and $d\mathbf{y}_2$ on S_t under the deformation. Obviously, the line elements are tangential to the surface.

The transformation of the surface element is given by the following equation (*Nanson's formula*)

$$\mathbf{n}dA_t = J\mathbf{F}^{-T}\mathbf{m}dA \quad (\text{A.15})$$

where \mathbf{n} denotes versor normal to the surface element dA_t (deformed configuration) and \mathbf{m} denotes versor normal to surface element dA (reference configuration).

The transformation law for the volume elements is simply

$$dV_t = JdV. \quad (\text{A.16})$$

Hence we conclude that J is a measure of the change in volume under the deformation. The deformation is said to be *isochoric* if there is no change in volume, i.e.

$$J \equiv \det \mathbf{F} = 1. \tag{A.17}$$

A material for which (A.17) holds for *all deformations* is called an *incompressible material*.

Let \mathbf{F} be the deformation gradient, $\det \mathbf{F} > 0$. There exist unique, positive definite, symmetric tensors, \mathbf{U} and \mathbf{V} , and a unique proper orthogonal tensor \mathbf{R} such that

$$\mathbf{F} = \mathbf{R}\mathbf{U} = \mathbf{V}\mathbf{R}. \tag{A.18}$$

The last relation is called the *polar decomposition theorem*.

Since \mathbf{U} is positive definite and symmetric there exist unique eigenvectors $\mathbf{u}^{(i)}$ such that

$$\mathbf{U} = \lambda_i \mathbf{u}^{(i)} \otimes \mathbf{u}^{(i)} = \lambda_1 \mathbf{u}^{(1)} \otimes \mathbf{u}^{(1)} + \lambda_2 \mathbf{u}^{(2)} \otimes \mathbf{u}^{(2)} + \lambda_3 \mathbf{u}^{(3)} \otimes \mathbf{u}^{(3)} \tag{A.19}$$

where $\lambda_i > 0$ are the *principal stretches* of the deformation and $\mathbf{u}^{(i)}$ are the *principal directions*; obviously, $\lambda_i = \lambda(\mathbf{u}^{(i)})$. Simple calculation shows that $\lambda_i > 0$ and λ_i are also the eigenvalues of \mathbf{V} with eigenvectors $\mathbf{R}\mathbf{u}^{(i)}$.

Now we proceed to introducing the notion of *stretch*, *extension*, *shear* and *strain*. Let \mathbf{c} and \mathbf{d} be unit vectors along $d\mathbf{x}$ and $d\mathbf{y}$ respectively, so that $d\mathbf{x} = \mathbf{c}|d\mathbf{x}|$, $d\mathbf{y} = \mathbf{d}|d\mathbf{y}|$ and (A.9) yields $\mathbf{d}|d\mathbf{y}| = \mathbf{F}\mathbf{c}|d\mathbf{x}|$. Hence

$$|d\mathbf{y}|^2 = (\mathbf{F}\mathbf{c}) \cdot (\mathbf{F}\mathbf{c})|d\mathbf{x}|^2 = (\mathbf{F}^T \mathbf{F}\mathbf{c}) \cdot \mathbf{c}|d\mathbf{x}|^2. \tag{A.20}$$

The last relation gives

$$\frac{|d\mathbf{y}|}{|d\mathbf{x}|} = |\mathbf{F}\mathbf{c}| = [\mathbf{c} \cdot (\mathbf{F}^T \mathbf{F}\mathbf{c})]^{1/2} \equiv \lambda(\mathbf{c}), \tag{A.21}$$

which defines $\lambda(\mathbf{c})$, called the *stretch in the direction* \mathbf{c} at \mathbf{x} . We observe that $0 < \lambda(\mathbf{c}) < +\infty$ for all unit vectors \mathbf{c} .

Take now a pair of line elements dx_1, dx_2 based at \mathbf{x} so that

$$dy_1 = \mathbf{F}dx_1, \quad dy_2 = \mathbf{F}dy_2.$$

Let θ denote the angle between them and ϑ the corresponding angle after deformation. Then

$$\cos \theta = \mathbf{c}_1 \cdot \mathbf{c}_2, \quad \cos \vartheta = \frac{(\mathbf{F}\mathbf{c}_1) \cdot (\mathbf{F}\mathbf{c}_2)}{\lambda(\mathbf{c}_1)\lambda(\mathbf{c}_2)}.$$

The change in angle $\theta - \vartheta$ (which may be positive or negative) is called the *shear* of the directions $\mathbf{c}_1, \mathbf{c}_2$ in the plane of $\mathbf{c}_1\mathbf{c}_2$.

Furthermore, from (A.20) we get

$$|d\mathbf{y}|^2 - |d\mathbf{x}|^2 = d\mathbf{x} \cdot (\mathbf{F}^T\mathbf{F} - \mathbf{I})d\mathbf{x}. \tag{A.22}$$

The material is said to be unstrained at \mathbf{x} if no line element changes length, i.e.,

$$d\mathbf{x} \cdot (\mathbf{F}^T\mathbf{F} - \mathbf{I})d\mathbf{x} = 0 \quad \forall d\mathbf{x},$$

or, equivalently,

$$\lambda(\mathbf{c}) = 1 \quad \text{for all unit vectors } \mathbf{c}.$$

It follows that $\mathbf{F}^T\mathbf{F} - \mathbf{I} = \mathbf{0}$, the zero tensor. Then \mathbf{F} is just a rotation \mathbf{R} , since, for orthogonal \mathbf{R} , we have $\mathbf{R}^T\mathbf{R} = \mathbf{I}$.

Strain is measured locally by changes in the lengths of line elements, i.e., by the value of (A.22). Thus, the tensor $\mathbf{F}^T\mathbf{F} - \mathbf{I}$ is a *measure of strain*. The so-called *Green strain tensor* \mathbf{E} is defined by

$$\mathbf{E} = \frac{1}{2}(\mathbf{F}^T\mathbf{F} - \mathbf{I}). \tag{A.23}$$

Using the polar decomposition (A.18) for the deformation gradient \mathbf{F} , we may also form the following tensor measures of deformation:

$$\mathbf{C} = \mathbf{F}^T\mathbf{F} = \mathbf{U}^2, \quad \mathbf{B} = \mathbf{F}\mathbf{F}^T = \mathbf{V}^2. \tag{A.24}$$

We refer to \mathbf{C} and \mathbf{B} as the *right* and *left Cauchy-Green deformation tensors*, respectively. Then \mathbf{E} may be written as follows:

$$\mathbf{E} = \frac{1}{2}(\mathbf{C} - \mathbf{I}) = \frac{1}{2}(\mathbf{U}^2 - \mathbf{I}). \tag{A.25}$$

The tensors \mathbf{U} and \mathbf{V} are called the *right* and *left stretch tensors*, respectively. We observe that the deformation \mathbf{F} rotates the principal axes of \mathbf{U} into those of \mathbf{V} as well as consists of stretching along those directions. The principal axes of \mathbf{U} and \mathbf{V} are often referred to as the *Lagrangian* and *Eulerian* principal axes, respectively.

In fact, one may define an infinite family of strain measures based on \mathbf{U} . For instance, we define $\mathbf{E}^{(m)}$ as follows:

$$\mathbf{E}^{(0)} = \ln \mathbf{U} \quad \text{if } m = 0, \tag{A.26}$$

$$\mathbf{E}^{(m)} = \frac{1}{m}(\mathbf{U}^m - \mathbf{I}) \quad \text{if } m \neq 0, \tag{A.27}$$

where m is a real number, not necessarily an integer. These are Lagrangian tensors, all coaxial with \mathbf{U} , and having eigenvalues $\ln \lambda_i$ for $m = 0$ and $(\lambda_i^m - 1)/m$ for $m \neq 0$. Corresponding Eulerian tensors $\mathbf{e}^{(m)}$ are based on \mathbf{V} and are defined by

$$\mathbf{e}^{(0)} = \ln \mathbf{V} \quad \text{if } m = 0, \tag{A.28}$$

$$\mathbf{e}^{(m)} = \frac{1}{m}(\mathbf{V}^m - \mathbf{I}) \quad \text{if } m \neq 0. \tag{A.29}$$

We observe that, on recalling the connection $\mathbf{V} = \mathbf{RUR}^T$, $\mathbf{e}^{(m)} = \mathbf{RE}^{(m)}\mathbf{R}^T$ for each m . Consequently, $\mathbf{E}^{(m)}$ and $\mathbf{e}^{(m)}$ have the same eigenvalues.

The reader probably noticed that we use interchangeably the expressions “strain tensor” and “strain measure”, like many authors do.

Let us recall that the *displacement vector* \mathbf{u} of a particle is defined as follows:

$$\mathbf{u} = \mathbf{y} - \mathbf{x}. \tag{A.30}$$

Hence

$$\mathbf{y} = \mathbf{x} + \mathbf{u}$$

and

$$\mathbf{F} = \nabla_{\mathbf{x}}\mathbf{y} = \mathbf{I} + \nabla_{\mathbf{x}}\mathbf{u}. \tag{A.31}$$

Here $\nabla_{\mathbf{x}}\mathbf{u}$ is the *displacement gradient*.

Analysis of motion

Previously, the velocity has been introduced and denoted by \mathbf{v} . The *velocity gradient* \mathbf{L} is defined by

$$\mathbf{L} = \nabla_{\mathbf{y}}\mathbf{v}. \tag{A.32}$$

It can be verified that the following identities hold

$$\dot{\mathbf{F}} = \mathbf{L}\mathbf{F}. \tag{A.33}$$

$$\dot{J} = \frac{\partial}{\partial t}(\det \mathbf{F}) = J \operatorname{tr} \mathbf{L} = J L_{ii} = J \operatorname{div}_{\mathbf{y}}\mathbf{v} = J \frac{\partial v_i}{\partial y_i}. \tag{A.34}$$

Hence we conclude that $\operatorname{div}_{\mathbf{y}}\mathbf{v}$ measures the rate at which volume changes during the motion. Consider an isochoric motion: $J \equiv 1$, $\dot{J} = 0$; consequently

$$\operatorname{div}_{\mathbf{y}}\mathbf{v} = 0.$$

Let us set

$$\mathbf{L} = \mathbf{D} + \mathbf{W}, \quad (\text{A.35})$$

where

$$\mathbf{D} = \frac{1}{2}(\mathbf{L} + \mathbf{L}^T), \quad \mathbf{W} = \frac{1}{2}(\mathbf{L} - \mathbf{L}^T). \quad (\text{A.36})$$

\mathbf{D} is called the (*Eulerian*) *strain-rate tensor* or *rate of stretching tensor*. Obviously, the motion is rigid if and only if $\mathbf{D} = \mathbf{0}$.

We have

$$\frac{\partial}{\partial t}(dy) = \frac{\partial}{\partial t}(\mathbf{F}dx) = \dot{\mathbf{F}}dx = \mathbf{L}Fdx = \mathbf{L}dy = (\mathbf{D} + \mathbf{W})dy.$$

Let now $\mathbf{D} = \mathbf{0}$, so that

$$\frac{\partial}{\partial t}dy = \mathbf{W}dy = \mathbf{w} \times dy \quad (\text{A.37})$$

where \mathbf{w} is the axial vector of \mathbf{W} , i.e.,

$$w_i = \varepsilon_{ijk}W_{jk}.$$

Here (ε_{ijk}) is the permutation or orientation symbol.

Formula (A.37) shows that in this specific case ($\mathbf{D} = \mathbf{0}$) the motion is locally a rigid rotation and \mathbf{W} is a measure of the *rate of rotation* (or *spin*) of line elements and it is called the *body spin*. The sum of \mathbf{D} and \mathbf{W} shows that the motion consists of stretching and rotation (similar to the interpretation of \mathbf{U} and \mathbf{R}). However, if $\mathbf{D} \neq \mathbf{0}$ then it contributes a rotation to line elements and the interpretation of \mathbf{W} requires modification, cf. Ogden [46].

B. Balance Laws, Field Equations and Stress

Let R_t be an arbitrary region in the current configuration Ω_t . Under the assumption of no mass transfer, as R_t moves it always consists of the same material, so its mass does not change, i.e.,

$$\frac{d}{dt} \int_{R_t} \rho dV_t = 0. \quad (\text{B.1})$$

The last equation presents one form of the *conservation of mass equation*. To derive the *local equation*, we use one of transport formulas. Let ϕ be a scalar field defined on Ω_t , and particularly on R_t . We have

$$\frac{d}{dt} \int_{R_t} \phi dV_t = \int_{R_t} (\dot{\phi} + \phi \operatorname{tr} \mathbf{L}) dV_t = \int_{R_t} (\dot{\phi} + \phi \operatorname{div}_y \mathbf{v}) dV_t. \quad (\text{B.2})$$

Applying (B.2) to (B.1) and noting that R_t is arbitrary, we obtain

$$\dot{\rho} + \rho \operatorname{div}_{\mathbf{y}} \mathbf{v} = 0. \tag{B.3}$$

This equation is known as the *continuity equation*. Recalling that, see Eq. (A.12),

$$\dot{\rho} = \frac{D\rho}{Dt} = \frac{\partial\rho}{\partial t} + \mathbf{v} \cdot \nabla_{\mathbf{y}}\rho,$$

Eq. (B.3) is transformed into an equivalent form

$$\frac{\partial\rho}{\partial t} + \operatorname{div}_{\mathbf{y}}(\rho\mathbf{v}) = 0. \tag{B.4}$$

Recall, from (A.34), that $\dot{J} = J \operatorname{div}_{\mathbf{y}} \mathbf{v}$. Substitution for $\operatorname{div}_{\mathbf{y}} \mathbf{v}$ from (B.3) then gives $\rho\dot{J} + \dot{\rho}J = 0$. Hence $\partial(\rho J)/\partial t = 0$. In the reference configuration $J = 1$ so that $\rho J = \rho^0$, where ρ^0 is the mass density in the reference configuration. Thus,

$$\rho = J^{-1}\rho^0. \tag{B.5}$$

The concepts of force and torque describe the action of a moving body \mathcal{B} on its surroundings and the mutual actions of the parts of \mathcal{B} on each other. With $R_t \subset \Omega_t$ we associate two vectors, $\mathbf{F}(R_t)$ and $\mathbf{G}(R_t; \mathcal{O})$, called the *force* and *torque* with respect to origin \mathcal{O} on the material in R_t . In general two types of force and torque must be accounted for. These are *body forces* and *body torques*, which act on the particles of a body (arising from gravity or magnetic fields, for example), and *contact forces* and *contact torques* resulting from the action of one part of the body on another across a separating surface (for example, pressure, friction or adhesion).

The body force and torque, measured *per unit mass*, are denoted \mathbf{b} and \mathbf{c} , respectively. Their contributions to $\mathbf{F}(R_t)$ and $\mathbf{G}(\mathbf{R}; \mathcal{O})$ are

$$\int_{R_t} \rho \mathbf{b} \, dV_t, \quad \int_{R_t} [\mathbf{y} \times (\rho \mathbf{b}) + \rho \mathbf{c}] \, dV_t,$$

respectively, where \mathbf{y} is the position vector of the point at which \mathbf{b} acts.

A mathematical description of contact forces (but not torques) relies on *Cauchy's stress principle*, which is regarded as an axiom. This states that

the action of the material occupying that part of Ω_t exterior to a closed surface S_t on the material occupying the interior part is represented by a vector field, denoted $\mathbf{t}(\mathbf{n}, \mathbf{y})$, defined on S_t and with physical dimensions of force per unit area.

We refer to \mathbf{t} as the *Cauchy stress vector*.

For nonpolar materials the total force and total torque (sometimes referred to as couple) about \mathcal{O} acting on R_t are given by

$$\mathbf{R}(R_t) = \int_{R_t} \rho \mathbf{b} \, dV_t + \int_{\partial R_t} \mathbf{t} \, dA_t, \quad (\text{B.6})$$

$$\mathbf{G}(R_t; \mathcal{O}) = \int_{R_t} \rho (\mathbf{y} \times \mathbf{b} + \mathbf{c}) \, dV_t + \int_{\partial R_t} \mathbf{y} \times \mathbf{t} \, dA_t. \quad (\text{B.7})$$

The *linear momentum* of the material occupying $R_t \subset \Omega_t$ is defined as

$$\mathbf{M}(R_t) = \int_{R_t} \rho \mathbf{v} \, dV_t. \quad (\text{B.8})$$

With respect to an origin \mathcal{O} , the *angular momentum* of the material occupying R_t is defined as

$$\mathbf{H}(R_t; \mathcal{O}) = \int_{R_t} \mathbf{y} \times (\rho \mathbf{v}) \, dV_t. \quad (\text{B.9})$$

B.1. Euler's Laws of Rotation

Euler's laws of motion are defined by

$$\frac{d\mathbf{M}}{dt} = \mathbf{F}, \quad \frac{d\mathbf{H}}{dt} = \mathbf{G}. \quad (\text{B.10})$$

They parallel Newton's laws for particles and rigid bodies. There is, however, a difference. In classical mechanics (B.10)₂ is a consequence of (B.10)₁, whereas in continuum mechanics this is not the case and the two equations in (B.10) are independent.

To write (B.10) in an explicit manner one needs the following transport formula

$$\frac{d}{dt} \int_{R_t} \mathbf{u} \, dV_t = \int_{R_t} [\dot{\mathbf{u}} + (\text{tr} \mathbf{L}) \mathbf{u}] \, dV_t \quad (\text{B.11})$$

which holds for any vector field \mathbf{u} .

Setting $\mathbf{c} = \mathbf{0}$ and applying (B.11) to (B.10)₁ with $\mathbf{u} = \rho \mathbf{v}$ and taking into account (B.3) we obtain

$$\int_{R_t} \rho (\mathbf{a} - \mathbf{b}) \, dV_t = \int_{\partial R_t} \mathbf{t} \, dA_t, \quad (\text{B.12})$$

where $\mathbf{a} = \dot{\mathbf{v}}$ denotes the acceleration.

Similarly from (B.10)₂ we get

$$\int_{R_t} \rho \mathbf{y} \times (\mathbf{a} - \mathbf{b}) dV_t = \int_{\partial R_t} \mathbf{y} \times \mathbf{t} dA_t. \quad (\text{B.13})$$

Note that $\mathbf{v} \times \mathbf{v} = \mathbf{0}$.

B.2. Cauchy Stress Tensor

Let (\mathbf{t}, \mathbf{b}) be a system of surface (contact) and body forces for \mathcal{B} during a motion. A *necessary and sufficient condition* for the momentum balance equations (B.12) and (B.13) to be satisfied is that there exists a second order tensor $\boldsymbol{\sigma} = (\sigma_{ij})$, called the Cauchy stress tensor, such that

(a) for each unit vector \mathbf{n} ,

$$\mathbf{t}(\mathbf{n}, \mathbf{x}) = \boldsymbol{\sigma}(\mathbf{y})\mathbf{n}(\mathbf{y}), \quad (\text{B.14})$$

where $\boldsymbol{\sigma}$ is independent of \mathbf{n} ,

(b) the tensor $\boldsymbol{\sigma}$ is symmetric, i.e.,

$$\boldsymbol{\sigma}^T = \boldsymbol{\sigma}, \quad (\text{B.15})$$

(c) $\boldsymbol{\sigma}$ satisfies the *equation of motion*

$$\rho \mathbf{a} = \text{div}_{\mathbf{y}} \boldsymbol{\sigma} + \rho \mathbf{b}. \quad (\text{B.16})$$

B.3. Energy Balance Equation

This equation has the following form

$$P_e(R_t) = \frac{d}{dt} K(R_t) + P_{in}(R_t). \quad (\text{B.17})$$

Here $P_e(R_t)$ denotes the rate of working, or *power*, of the forces acting on R_t defined by

$$P_e(R_t) = \int_{R_t} \rho \mathbf{b} \cdot \mathbf{v} dV_t + \int_{\partial R_t} \mathbf{t} \cdot \mathbf{v} dA_t. \quad (\text{B.18})$$

The *kinetic energy* $K(R_t)$ of the material occupying R_t is defined as follows

$$K(R_t) = \frac{1}{2} \int_{R_t} \rho \mathbf{v} \cdot \mathbf{v} \, dV_t \quad (\text{B.19})$$

and

$$P_{in}(R_t) = \int_{R_t} \text{tr}(\boldsymbol{\sigma} \mathbf{D}) \, dV_t. \quad (\text{B.20})$$

From (B.17) we conclude that the power of forces acting on R_t is converted into kinetic energy and $P_{in}(R_t)$. The latter may consist of stored (or potential) energy or be a measure of the amount of work dissipated in the form of heat or be a mixture of the two.

C. Conjugate Pairs of Stress and Strain Tensors

Using Nanson's formula (A.15) the traction on an area element $\mathbf{n} dA_t$ in the current configuration can be written as follows

$$\mathbf{t} \, dA_t = \boldsymbol{\sigma} \mathbf{n} \, dA_t = J \boldsymbol{\sigma} \mathbf{F}^{-T} \mathbf{m} \, dA \equiv \mathbf{P} \mathbf{m} \, dA, \quad (\text{C.1})$$

wherein the first (unsymmetric) *Piola-Kirchoff* stress tensor is defined by

$$\mathbf{P} = J \boldsymbol{\sigma} \mathbf{F}^{-T}. \quad (\text{C.2})$$

The first Piola-Kirchoff stress tensor measures the force per *unit reference area* while $\boldsymbol{\sigma}$ measures the force per *unit deformed area*.

The symmetry of $\boldsymbol{\sigma}$ gives

$$\mathbf{P} \mathbf{F}^T = \mathbf{F} \mathbf{P}^T. \quad (\text{C.3})$$

The equation of motion (B.16) can be written in terms of \mathbf{P}

$$\text{div}_x \mathbf{P} + \rho^0 \mathbf{b} = \rho^0 \dot{\mathbf{v}}. \quad (\text{C.4})$$

Alternatively, the identity $\text{div}_y (J^{-1} \mathbf{F}) = \mathbf{0}$, obtained from (A.14)₄ by setting $\mathbf{T} = \mathbf{I}$, can be used to give

$$\text{div}_y \boldsymbol{\sigma} = J^{-1} \text{div}_x \mathbf{P}.$$

In the reference configuration the integral for P_{in} becomes

$$\int_R J \text{tr}(\boldsymbol{\sigma} \mathbf{D}) \, dV. \quad (\text{C.5})$$

The last integrand presents the *rate of working of the stresses per unit reference volume*, i.e., the stress power density. Using the symmetry of $\boldsymbol{\sigma}$ together with (A.32), (A.33) and (C.2) we obtain

$$J \operatorname{tr}(\boldsymbol{\sigma} \mathbf{D}) = J \operatorname{tr}(\boldsymbol{\sigma} \mathbf{L}) = \operatorname{tr}(\mathbf{F} \mathbf{P}^T \mathbf{L}) = \operatorname{tr}(\mathbf{P}^T \mathbf{L} \mathbf{F}) = \operatorname{tr}(\mathbf{P}^T \dot{\mathbf{F}}) = \operatorname{tr}(\mathbf{S} \dot{\mathbf{F}}). \tag{C.6}$$

Hence we conclude that the stress power is also given by $\operatorname{tr}(\mathbf{S} \dot{\mathbf{F}})$. We say that \mathbf{S} and \mathbf{F} consistute a pair of *conjugate* stress and deformation tensors.

Furthermore, by setting $\mathbf{E} = \mathbf{E}^{(2)}$ we write

$$\mathbf{E}^{(2)} = \frac{1}{2}(\mathbf{F}^T \mathbf{F} - \mathbf{I}).$$

Hence, by using (A.33) we get

$$\dot{\mathbf{E}}^{(2)} = \frac{1}{2}(\mathbf{F}^T \dot{\mathbf{F}} + \dot{\mathbf{F}}^T \mathbf{F}) \equiv \mathbf{F}^T \mathbf{D} \mathbf{F}. \tag{C.7}$$

The stress power is written as

$$\operatorname{tr}(\mathbf{P}^T \dot{\mathbf{F}}) = \operatorname{tr}(\mathbf{S} \dot{\mathbf{F}}) = \operatorname{tr}(\mathbf{S} \mathbf{F}^{-T} \mathbf{F}^T \dot{\mathbf{F}}) = \operatorname{tr}(\mathbf{S} \mathbf{F}^{-T} \dot{\mathbf{E}}^{(2)}) = \operatorname{tr}(\mathbf{T}^{(2)} \dot{\mathbf{E}}^{(2)}) \tag{C.8}$$

where

$$\mathbf{T}^{(2)} = \mathbf{S} \equiv \mathbf{S} \mathbf{F}^{-T} = J \mathbf{F}^{-1} \boldsymbol{\sigma} \mathbf{F}^{-T} \tag{C.9}$$

is the *second (symmetric) Piola-Kirchoff* stress tensor, i.e. $\mathbf{S} = \mathbf{S}^T$. The first and second Piola-Kirchoff stress tensors are related by

$$\mathbf{P} = \mathbf{F} \mathbf{S}. \tag{C.10}$$

The stress and strain pair $(\mathbf{T}^{(2)}, \mathbf{E}^{(2)})$ or (\mathbf{S}, \mathbf{E}) is a pair of conjugate stress and strain tensors.

The *Kirchoff stress tensor*, being the “weighted” Cauchy stress, is denoted by

$$\boldsymbol{\tau} = J \boldsymbol{\sigma}. \tag{C.11}$$

We already know that $\mathbf{F}^T \mathbf{F} = \mathbf{U}^2$, cf. (A.24)₁. Hence we also have

$$\dot{\mathbf{E}}^{(2)} = \frac{1}{2}(\mathbf{U} \dot{\mathbf{U}} + \dot{\mathbf{U}} \mathbf{U}).$$

Using the symmetry of $\mathbf{T}^{(2)}$ and of $\dot{\mathbf{U}}$ we obtain

$$\operatorname{tr}(\mathbf{T}^{(2)} \dot{\mathbf{E}}^{(2)}) = \operatorname{tr}(\mathbf{T}^{(2)} \mathbf{U} \dot{\mathbf{U}}) = \operatorname{tr}\left[\frac{1}{2}(\mathbf{T}^{(2)} \mathbf{U} + \mathbf{U} \mathbf{T}^{(2)}) \dot{\mathbf{U}}\right].$$

Thus we may introduce the definition of the *Biot stress tensor* $\mathbf{T}^{(1)}$, conjugate to the strain tensor

$$\mathbf{E}^{(1)} \equiv \mathbf{U} - \mathbf{I}, \quad (\text{C.12})$$

as

$$\mathbf{T}^{(1)} = \frac{1}{2}(\mathbf{T}^{(2)}\mathbf{U} + \mathbf{U}\mathbf{T}^{(2)}). \quad (\text{C.13})$$

Indeed, $\dot{\mathbf{E}}^{(1)} = \dot{\mathbf{U}}$ and consequently the stress and strain pair $(\mathbf{T}^{(1)}, \mathbf{E}^{(1)})$ constitute a pair of conjugate stress and strain tensors.

By using the polar decomposition (A.18), the Biot stress tensor takes the form

$$\mathbf{T}^{(1)} = \frac{1}{2}(\mathcal{S}\mathbf{R} + \mathbf{R}^T\mathcal{S}^T) = \frac{1}{2}(\mathbf{P}^T\mathbf{R} + \mathbf{R}^T\mathbf{P}). \quad (\text{C.14})$$

Summarizing, we have the connections

$$J \operatorname{tr}(\boldsymbol{\sigma}\mathbf{D}) = \operatorname{tr}(\mathcal{S}\dot{\mathbf{F}}) = \operatorname{tr}(\mathbf{T}^{(2)}\dot{\mathbf{E}}^{(2)}) = \operatorname{tr}(\mathbf{T}^{(1)}\dot{\mathbf{E}}^{(1)}). \quad (\text{C.15})$$

Moreover, $\mathcal{S} = \mathbf{P}^T$, $\mathbf{T}^{(2)} = \mathbf{S}$, and \mathbf{P} and \mathbf{S} denote the first and second Piola-Kirchoff stress tensor, respectively. The strain measure $\mathbf{E}^{(2)}$ is usually denoted by \mathbf{E} .

More generally, the symmetric stress tensor $\mathbf{T}^{(m)}$ conjugate to the strain tensor $\mathbf{E}^{(m)} \equiv (\mathbf{U}^{(m)} - \mathbf{I})/m$ may be defined via the identity

$$\operatorname{tr}(\mathbf{T}^{(m)}\dot{\mathbf{E}}^{(m)}) = \operatorname{tr}(\mathbf{T}^{(1)}\dot{\mathbf{E}}^{(1)}) = \operatorname{tr}(\mathbf{T}^{(1)}\dot{\mathbf{U}}). \quad (\text{C.16})$$

The limit case $m \rightarrow 0$ is much more complex and we will not discuss it here.

D. General Constitutive Relationships for Elastic Materials

This section presents an introduction to constitutive modeling of nonlinear elastic materials. We shall discuss isotropic, transversally isotropic and orthotropic materials. Inelastic materials will not be discussed, though contact problems with friction for finitely deformed plastic materials are of great practical interest.

Revival of interest in nonlinear elasticity is due to the development of rubber-like materials (see Dorfmann and Muhr, [15]) and constitutive modeling of soft tissues, cf. Holzapfel and Ogden [46], Jemioło and Telega [36].

D.1. General Relations

Let us first introduce the notion of *Cauchy elasticity*. A material is said to be elastic in the sense of Cauchy if it is described by the constitutive equation in the form, cf. Ciarlet [11], Ogden [45, 46],

$$\boldsymbol{\sigma} = \mathbf{g}(\mathbf{F}). \quad (\text{D.1})$$

Here \mathbf{g} is a *symmetric tensor valued function*, defined on the space of deformation gradients \mathbf{F} . We recall that $\boldsymbol{\sigma} = \boldsymbol{\sigma}^T$. Equation (D.1) states that the stress in Ω at a point \mathbf{x} depends only on the deformation gradient at \mathbf{x} and not on the history of deformation. In particular, it is independent of the path of deformation taken to reach the point \mathbf{F} . The function \mathbf{g} is referred to as the *Cauchy stress response function*.

The elastic material is called *homogeneous* if \mathbf{g} does not depend explicitly on $\mathbf{x} \in \Omega$. If it does, the material is *inhomogeneous*. For instance, \mathbf{g} may depend on \mathbf{x} if

$$\boldsymbol{\sigma} = \mathbf{g}(\rho^0(\mathbf{x}), \mathbf{F}). \quad (\text{D.2})$$

As previously, ρ^0 denotes the mass density in the reference configuration. Soft tissues as well as bone tissue are inhomogeneous biological material.

When the stress is removed the deformation vanishes, so that

$$\mathbf{g}(\mathbf{I}) = \mathbf{0}. \quad (\text{D.3})$$

It means that the underformed configuration is *free of stress*.

Condition (D.3) is not satisfied in the presence of residual stresses, like in soft tissues.

Suppose now that a rigid-body motion

$$\widehat{\mathbf{y}} = \mathbf{Q}(t)\mathbf{y} + \mathbf{c}(t) \quad (\text{D.4})$$

is superimposed on the motion $\mathbf{y} = \mathbf{y}(\mathbf{x}, t)$. Then the deformation gradient, $\widehat{\mathbf{F}}$ say, is given

$$\widehat{\mathbf{F}} = \mathbf{Q}\mathbf{F}. \quad (\text{D.5})$$

Indeed, since

$$\widehat{y}_i = Q_{ik}y_k + c_i,$$

we obtain

$$\frac{\partial \widehat{y}_i}{\partial y_k} = Q_{im} \frac{\partial y_m}{\partial y_k} = Q_{im} \delta_{mk} = Q_{ik},$$

and thus

$$\widehat{F}_{ij} = \frac{\partial \widehat{y}_i}{\partial x_j} = \frac{\partial \widehat{y}_i}{\partial y_k} \frac{\partial y_k}{\partial x_j} = Q_{ik} F_{kj}.$$

For an elastic material with response function \mathbf{g} , the stress tensor, $\widehat{\boldsymbol{\sigma}}$ say, associated with the deformation gradient $\widehat{\mathbf{F}}$ is

$$\widehat{\boldsymbol{\sigma}} = \mathbf{g}(\widehat{\mathbf{F}}).$$

Under the rotation \mathbf{Q} the unit normal to ∂R_t becomes $\widehat{\mathbf{n}} = \mathbf{Q}\mathbf{n}$ and the traction vector $\widehat{\mathbf{t}}$ becomes $\widehat{\mathbf{t}} = \mathbf{Q}\mathbf{t}$. Since $\mathbf{t} = \boldsymbol{\sigma}\mathbf{n}$, $\widehat{\mathbf{t}} = \widehat{\boldsymbol{\sigma}}\widehat{\mathbf{n}}$ we obtain

$$\mathbf{Q}\boldsymbol{\sigma}\mathbf{n} = \widehat{\boldsymbol{\sigma}}\mathbf{Q}\mathbf{n}.$$

This holds for arbitrary \mathbf{n} and hence

$$\widehat{\boldsymbol{\sigma}} = \mathbf{Q}\boldsymbol{\sigma}\mathbf{Q}^T.$$

The response function \mathbf{g} must therefore satisfy the *invariance requirement*

$$\mathbf{g}(\widehat{\mathbf{F}}) \equiv \mathbf{g}(\mathbf{Q}\mathbf{F}) = \mathbf{Q}\mathbf{g}(\mathbf{F})\mathbf{Q}^T \quad (\text{D.6})$$

for each \mathbf{F} and *all* rotations \mathbf{Q} . The last relation expresses the fact the constitutive equation (D.1) (and similarly (D.2)) is *objective*. For a deeper discussion, the reader is referred to Ciarlet [11], Ogden [45], [46, p. 47].

Let ϕ , \mathbf{u} , \mathbf{T} be scalar, vector and second-order tensor fields defined on Ω_t , i.e. they are Eulerian in character. Let $\widehat{\phi}$, $\widehat{\mathbf{u}}$, $\widehat{\mathbf{T}}$ be the corresponding fields on $\widehat{\Omega}_t$, where $\widehat{\Omega}_t$ is obtained from Ω_t by the rigid-body motion (D.4). The fields are said to be objective if, for all such motions,

$$\widehat{\phi} = \phi, \quad \widehat{\mathbf{u}} = \mathbf{Q}\mathbf{u}, \quad \widehat{\mathbf{T}} = \mathbf{Q}\mathbf{T}\mathbf{Q}^T. \quad (\text{D.7})$$

It can easily be verified that if ϕ is an objective scalar field then $\nabla_{\mathbf{y}}\phi$ is an objective vector field, i.e.

$$\nabla_{\widehat{\mathbf{y}}}\widehat{\phi} = \mathbf{Q}\nabla_{\mathbf{y}}\phi.$$

We note that neither the velocity nor acceleration are objective vectors.

D.2. Material Symmetry

Let \mathcal{G} be a subgroup of the full orthogonal group $\mathcal{O}(3)$. \mathcal{G} is called the *symmetry group* of the material relative to Ω if

$$\mathbf{g}(\mathbf{F}\mathbf{Q}) = \mathbf{g}(\mathbf{F}) \tag{D.8}$$

for all $\mathbf{Q} \in \mathcal{G}$. In the particular case, if \mathcal{G} is the proper orthogonal group then the material is said to be *isotropic relative to* Ω , and (D.8) holds for *all proper orthogonal* \mathbf{Q} (for every deformation gradient \mathbf{F}). Physically, this means that the response of a “small” specimen of material cut from Ω is independent of its orientation in Ω .

To find the general form of isotropic constitutive equation for a nonlinear isotropic material one may use the theory of representation of isotropic second-order symmetric *tensor functions*, cf. Jemioło and Telega [35], Zheng [81].

Let us apply this theory to isotropic elastic materials. From (D.8) we have

$$\boldsymbol{\sigma} = \mathbf{g}(\mathbf{F}) = \mathbf{g}(\mathbf{F}\mathbf{Q}) \tag{D.9}$$

for all proper orthogonal \mathbf{Q} and each deformation gradient \mathbf{F} .

The choice $\mathbf{Q} = \mathbf{R}^T$ and use of the polar decomposition $\mathbf{F} = \mathbf{V}\mathbf{R}$ in (D.9) yield

$$\boldsymbol{\sigma} = \mathbf{g}(\mathbf{V}).$$

We have

$$\mathbf{Q}\mathbf{g}(\mathbf{V})\mathbf{Q}^T = \mathbf{Q}\mathbf{g}(\mathbf{F})\mathbf{Q}^T = \mathbf{g}(\mathbf{Q}\mathbf{F}).$$

Replacing \mathbf{F} by $\mathbf{Q}\mathbf{F}$ and \mathbf{Q} by $\mathbf{R}^T\mathbf{Q}^T$ and knowing that $\mathbf{F} = \mathbf{V}\mathbf{R}$ we get

$$\mathbf{Q}\mathbf{g}(\mathbf{V})\mathbf{Q}^T = \mathbf{g}(\mathbf{Q}\mathbf{V}\mathbf{Q}^T) \tag{D.10}$$

for all proper orthogonal \mathbf{Q} . However, since \mathbf{Q} occurs twice on each side of (D.10), allowing \mathbf{Q} to be improper orthogonal does not affect (D.10), which then states that $\mathbf{g}(\mathbf{V})$ is an *isotropic, second-order tensor function* of \mathbf{V} , cf. Jemioło and Telega [35], Zheng [81].

Note that for an isotropic elastic material, $\boldsymbol{\sigma} = \mathbf{g}(\mathbf{V})$ is *coaxial with* \mathbf{V} , i.e. with the Eulerian principal axes. According to the representation theory of isotropic tensor functions we have, cf. Jemioło and Telega [35], Zhang [81]

$$\boldsymbol{\sigma} = \mathbf{g}(\mathbf{V}) = \phi_0\mathbf{I} + \phi_1\mathbf{V} + \phi_2\mathbf{V}_2, \tag{D.11}$$

where ϕ_0, ϕ_1, ϕ_2 are scalar (invariant) functions of \mathbf{V} , i.e. functions of

$$\begin{aligned} I_1 &= \lambda_1 + \lambda_2 + \lambda_3 = \operatorname{tr} \mathbf{V}, & I_2 &= \lambda_1 \lambda_2 + \lambda_2 \lambda_3 + \lambda_1 \lambda_3, \\ I_3 &= \lambda_1 \lambda_2 \lambda_3. \end{aligned}$$

We may also write

$$\boldsymbol{\sigma} = \sum_{i=1}^3 \sigma_i \mathbf{v}^{(i)} \otimes \mathbf{v}^{(i)},$$

where

$$\sigma_i = \phi_0 + \phi_1 \lambda_i + \phi_2 \lambda_i^2, \quad i = 1, 2, 3.$$

D.3. Hyperelastic Materials

The energy balance equation can be written in the form

$$\int_{R_t} \rho \mathbf{b} \cdot \mathbf{v} \, dV_t + \int_{\partial R_t} \mathbf{t} \cdot \mathbf{v} \, dA_t = \frac{d}{dt} \int_{R_t} \frac{1}{2} \rho \mathbf{v} \cdot \mathbf{v} \, dV_t + \int_{R_t} \operatorname{tr}(\boldsymbol{\sigma} \mathbf{D}) \, dV_t. \quad (\text{D.12})$$

If there is no dissipation then the work done by the body and surface forces is converted into kinetic energy and stored elastic energy. Thus a natural need for an interpretation of the second term on the right-hand side of (D.12) arises. We have

$$\int_{R_t} \operatorname{tr}(\boldsymbol{\sigma} \mathbf{D}) \, dV_t = \int_R J \operatorname{tr}(\boldsymbol{\sigma} \mathbf{D}) \, dV.$$

Recall that $\operatorname{tr}(\boldsymbol{\sigma} \mathbf{D}) = \operatorname{tr}(\boldsymbol{\sigma} \mathbf{L})$; then, the integrand $J \operatorname{tr}(\boldsymbol{\sigma} \mathbf{L})$ is interpreted as the rate of increase of elastic energy per unit volume in Ω .

Thus it is natural to introduce the elastic stored energy $W(\mathbf{F})$ per unit volume in Ω such that

$$\frac{\partial}{\partial t} W(\mathbf{F}) = J \operatorname{tr}(\boldsymbol{\sigma} \mathbf{L}). \quad (\text{D.13})$$

We observe that $W(\mathbf{F})$ is also referred to as the *strain energy* or *potential energy* per unit volume in Ω . Then, we get

$$\int_{R_t} \operatorname{tr}(\boldsymbol{\sigma} \mathbf{D}) \, dV_t = \int_R \frac{\partial}{\partial t} W(\mathbf{F}) \, dV = \frac{d}{dt} \int_R W(\mathbf{F}) \, dV.$$

The integral

$$\int_R W(\mathbf{F}) \, dV$$

is the total elastic strain energy in the region R . The right-hand side of (D.12) can now be written as follows

$$\frac{d}{dt}(\text{kinetic energy} + \text{strain energy}).$$

Since $\dot{\mathbf{F}} = \mathbf{L}\mathbf{F}$ and W depends only on \mathbf{F} (and on \mathbf{x} for inhomogeneous materials), we have

$$\frac{\partial}{\partial t}W(\mathbf{F}) = \frac{\partial W}{\partial F_{ij}} \frac{\partial F_{ij}}{\partial t} = \text{tr}\left(\frac{\partial W}{\partial \mathbf{F}} \dot{\mathbf{F}}^T\right) = \frac{\partial W}{\partial F_{ij}} L_{ik} F_{kj} = \text{tr}\left[\mathbf{F}\left(\frac{\partial W}{\partial \mathbf{F}}\right)^T \mathbf{L}\right].$$

Comparison of this with (D.13) yields

$$J\boldsymbol{\sigma} = \mathbf{F}\left(\frac{\partial W}{\partial \mathbf{F}}\right)^T. \quad (\text{D.14})$$

Recalling that $\boldsymbol{\sigma} = \mathbf{g}(\mathbf{F})$ we get

$$\mathbf{g}(\mathbf{F}) = J^{-1}\mathbf{F}\left(\frac{\partial W}{\partial \mathbf{F}}\right)^T. \quad (\text{D.15})$$

Taking into account the relation (C.2) between the Cauchy stress $\boldsymbol{\sigma}$ and the first Piola-Kirchhoff stress \mathbf{P} we readily obtain

$$\mathbf{P} = \frac{\partial W}{\partial \mathbf{F}}. \quad (\text{D.16})$$

An elastic material which possesses a stored energy function W is said to be *hyperelastic* or *Green elastic* material.

Note that the strain-energy function W may be isotropic or anisotropic, depending on material.

D.4. Objectivity of W

The stored energy function W is a scalar function. In this case objectivity requires that it is unaffected by a superimposed rigid-body rotation after deformation, i.e.,

$$W(\mathbf{Q}\mathbf{F}) = W(\mathbf{F}) \quad (\text{D.17})$$

for all rotations \mathbf{Q} for each deformation gradient \mathbf{F} . In other words, W is indifferent to observer transformation.



Already appeared in the ABIOMED *Lecture Notes* series:

1. J. MIZRAHI, *Muscle/Bone Interactions in the Musculo-Skeletal System*
2. A. NOWICKI and J. LITNIEWSKI (Eds.), *Proceedings of the Workshop on Ultrasound in Biomeasurements, Diagnostics and Therapy*



55765

INSTITUTE OF FUNDAMENTAL TECHNOLOGICAL RESEARCH
publishes the following periodicals:

- ARCHIVES OF MECHANICS — bimonthly (in English)
ARCHIVES OF ACOUSTICS — quarterly (in English)
ARCHIVES OF CIVIL ENGINEERING — quarterly (in English)
ENGINEERING TRANSACTIONS — quarterly (in English)
COMPUTER ASSISTED MECHANICS AND ENGINEERING SCIENCES
— quarterly (in English)
JOURNAL OF TECHNICAL PHYSICS — quarterly (in English)

Subscription orders for all journals edited by IFTR may be sent directly to:

Editorial Office

Institute of Fundamental Technological Research

Świętokrzyska 21, p. 508

00-049 Warszawa, POLAND